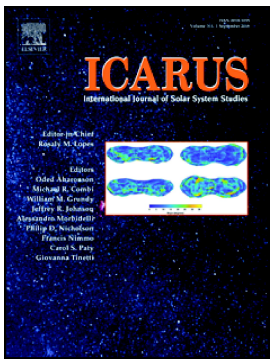

Equilibrium sediment transport, grade and discharge for suspended-load-dominated flows on Earth, Mars and Titan

Lawrence Amy, Robert Dorrell

PII: S0019-1035(20)30571-6

DOI: https://doi.org/10.1016/j.icarus.2020.114243

Reference: YICAR 114243

To appear in: *Icarus*

Received date: 7 July 2020

Revised date: 30 November 2020

Accepted date: 1 December 2020

Please cite this article as: L. Amy and R. Dorrell, Equilibrium sediment transport, grade and discharge for suspended-load-dominated flows on Earth, Mars and Titan, *Icarus* (2018), https://doi.org/10.1016/j.icarus.2020.114243

Equilibrium sediment transport, grade and discharge for suspended-load-dominated flows on Earth, Mars and Titan

Lawrence Amy[1] & Robert Dorrell[2]

[1]School of Earth Sciences, University College Dublin, Belfield, Dublin 4, Ireland.

[2]Energy and Environment Institute, University of Hull, Hull, HU6 7RX.

Abstract

Recent surface observations have emphasised the importance of bedload transport by rivers and streams on Mars and Titan. Previous "hydraulic" analysis, however, has also shown that transport as suspended load should be possible, if not more prevalent due to lower critical shear stresses, under reduced gravity conditions compared with Earth; where the dominant mode of sediment flux by rivers is as suspended load. A new suspended-load equilibrium condition (zero net erosion and deposition) constraint is advanced, using a flux-balance model applicable to transport (capacity) limited alluvial channels. The theory unifies Gilbert's relation for slope and flow capacity model with the Shields criterion for incipient motion. Shields-stress analysis shows that sediment transport thresholds on Earth, Mars and Titan are dynamically similar. Thus, despite large differences in dimensional shear stresses variations in the critical slopes and flow depths required for threshold and equilibrium conditions are comparatively modest. Under reduced gravity conditions, there exists a slightly higher potential for sediment transport as suspended load; except for systems involving high particle-fluid density ratios, as may apply to the transport of organic particles on Titan. Critically we show that graded suspended-load channels should develop gentler slopes under reduced gravity, and *not* steeper slopes as previously inferred based on generalized hydraulic geometry relationships of terrestrial river and submarine channels. We further argue that the use of submarine channels as analogues for channels formed under reduced gravity is physically not justified. Finally, compared

with bedload channels, suspended-load channels should also have markedly higher discharges, with implications for mechanistic-based discharge predictions and precipitation models.

Keywords: *Geomorphology, Equilibrium, Grade, Mars, Titan*

1. Introduction

Sediment transport by liquid geophysical flows is one of the primary processes responsible for reshaping the surface of planetary bodies. On Earth this process is widely expressed in the form of river drainage systems and their alluvial deposits, which dominate the geomorphology of large areas of the terrestrial surface and are responsible for the majority of sediment flux from land to oceans (Leopold & Wolman, 1957; Milliman & Meade, 1983; Syvitski et al., 2003; Giachetta & Willett, 2018). River and streams capable of moving sediment are also inferred, based on satellite and surface observational data, to have been important for sculpting the present or past surfaces of a number of other planetary bodies in the solar system, notably Mars and Saturn's moon Titan (Grotzinger et al., 2013; McSween et al., 2019).

The fundamental characteristics of rivers, such as how much sediment they transport and their morphology and equilibrium state, is linked to the manner in which they move sediment (as bedload, suspended load or a mixture of both), as governed by the imposed hydraulic and sedimentary conditions (Dade & Friend, 1998; Church, 2006). Equilibrium critically defines the boundary between erosional and depositional regimes and determines the "stable" state, encapsulated by the concept of a "graded" river, to which an alluvial channel will attempt to adjust through time (Lacey, 1930; Mackin, 1948; Dade & Friend, 1998). Whilst satellite and surface based observations from Mars and Titan, in many cases, suggest coarse-grained bedload-dominated systems, on Earth suspended load is the dominant mode of transport in terms of sediment flux,

accounting for the vast majority (~90%) of sediment moved by rivers (Milliman & Meade, 1983; Syvitski et al., 2003; Turowski et al., 2010).

Sediment-transport systems on the surfaces of Earth, Mars and Titan involve different types of fluid-particle systems and occur under different strengths of gravitational acceleration. Having a smaller mass, Mars and Titan have a reduced gravitational acceleration compared with Earth. Systems on ancient Mars are inferred to have involved flows of water or brines, transporting dominantly basaltic material (Carr, 2012; Lamb et al., 2012). Titan's volatile cycle involves hydrocarbons with surface flows of liquid methane or ethane that transport water-ice and organic particles (Lunine et al., 1983; Ori et al., 1998; Burr et al., 2013; Hayes et al., 2018). Accordingly, the physical conditions under which sediment transport occurs vary on different planetary bodies, with implications for our understanding of planetary surface processes, geomorphology, climate and planetary evolution (Miller & Komar, 1977; Komar, 1980; Burr et al., 2006; 2013; Grotzinger et al. 2013). Previous work has used hydraulic theory to examine the thresholds of sediment motion and suspension, and thus bedload and suspended load regimes, on Mars and Titan (e.g., Miller & Komar, 1977; Komar, 1980; Burr et al., 2006; 2013; Grotzinger et al. 2013). This work has identified that there exists a higher potential for sediment transport as suspended load under reduced gravity conditions (Komar, 1980; Burr et al., 2006).

Here, we build on earlier analyses of sediment transport on extra-terrestrial planets, by re-examining the conditions under which firstly, suspended-load-dominated flow should prevail and secondly, suspended-load-dominated flows are at equilibrium (i.e. *zero net erosion and deposition*) on Mars and Titan. The analysis of equilibrium conditions in this work is based on a newly developed model, based on a set of one-dimensional advection-diffusion equations describing the turbulent mixing and settling of suspended particles, previously shown to provide better predictions compared with other equilibrium models (Dorrell et al., 2018). Previous analysis for sediment transport on Mars and Titan has principally presented sediment transport thresholds in terms of the dimensional

bed shear stress or shear velocity. We here additionally provide an analysis in terms of dimensionless shear stress (i.e., Shields number), that describes the ratio of the flow force acting on a stationary particle on the bed to its submerged weight. The Shields number allows a more holistic examination of the net effect of gravity and particle-fluid system properties, on the ability of flows to move sediment on different planetary bodies.

In section 2, we describe the fluvial systems of Mars and Titan including the physical characteristics of particles and fluids used in the subsequent analyses. In section 3, we define regime boundaries for sediment transport modes and review the potential for suspended-load-dominated flows on Mars and Titan. In section 4, we then introduce an equilibrium model for suspended-load-dominated flow and provide an analysis of equilibrium dimensional and nondimensional shear stress (section 4.1), equilibrium slope (section 4.2) and unit discharge (section 4.3). In section 5, we summarize and discuss the key findings and implications of this work.

2. Fluvial systems on Mars and Titan and their physical parameters

2.1 Rivers and streams on Mars and Titan

Mars displays compelling evidence for ancient fluvial systems that suggests an active hydrological cycle involving surface runoff that occurred in the early history of Mars during the Noachian and early Hesperian, > 3.5 billion years ago (Baker et al., 1991; Achille & Hynek, 2010; Andrews-Hanna & Lewis, 2011; Villanueva et al., 2015; Cardenas et al., 2017). Satellite imagery reveals valley networks (Hynek et al., 2010), "inverted" river channels (Burr et al., 2010), flood outflow channels (Carr, 1979; Rodriguez et al., 2015), alluvial fans (Moore & Howard, 2005; Jacobsen & Burr, 2017) and intercrater deltas (Wood, 2006; Schon et al., 2012) (**Figure 1A-B**). Satellite-based interpretations of fluvial systems on Mars are consistent with outcrop data collected by the Curiosity and Opportunity rovers

(Grotzinger et al. 2005; Williams et al., 2013; Dietrich et al. 2017; Edgar et al. 2017). Titan is the only planetary body in the Solar System, other than Earth, considered to have a present-day active volatile cycle involving surficial liquid flow (Lorenz et al., 2008; Hayes et al., 2018). Radar images show valley networks (**Figure 1C-D**), similar to their terrestrial counterparts (Lorenz et al., 2008; Burr et al., 2013; Hayes et al., 2018). Images from the Huygens landing site on Titan also provide evidence for sediment transport, showing rounded clastic sediment grains on the surface of what is interpreted as a dry river bed (Tomasko et al., 2005; Perron et al., 2006).

Evidence for the type of sediment transport mode on Titan is scarce with more information available for Mars albeit coming from outcrops of ancient deposits. It is generally assumed that Martian channels are gravel-bedded (e.g., Morgan & Craddock, 2019) as supported by remote and surface observations (Wood, 2006; Williams et al., 2013; Dietrich et al. 2017; Edgar et al., 2017) and thus dominated by bedload sediment transport dynamics. Nevertheless, given the availability of fine-grained sediment (Schieber et al., 2016), evidence for long transport systems (Grotzinger et al, 2012) and energetic flows (Komar, 1980), it is likely that some transport systems on Mars involved suspended-load-dominated flow. Exposed ("inverted") channels on Mars of the Aeolis/Zephyria Plana region (**Figure 1A-B**) display meandering forms with well-developed internal structure, similar to terrestrial meander bars or scroll bars (Burr et al., 2009; 2010; Matsubara et al., 2015). Whilst single-thread sinuous channels on Earth often carry sand and gravel as bedload and conversely many braided rivers carry substantial amounts of fine suspended load (Bridge & Demicco, 2008), the morphology of the Aeolis/Zephyria Plana channels is similar to the morphology of finer-grained, mixed-load or suspended-load channels on Earth (Schumm, 1985; Church, 2006; Matsubara et al., 2015). Grain-size estimates for Martian channels from satellite observation are problematic due to surface dust (Burr et al., 2010). However, the weathering patterns and thermal inertia of channel deposits at Aeolis Dorsa suggest they are composed of sand or fine gravel; giving rise to the interpretation that these meandering streams may have had high suspended loads (Matsubara et al., 2015). Fluvial deposits observed in Gale Crater include i) planar-laminated sandstones potentially

formed under upper-stage plane bed conditions and ii) cross-stratified sandstones likely formed by migrating subaqueous dunes (Edgar et al. 2017). On Earth, upper-stage plane beds are formed at relatively high flow conditions, during which sediment is predominantly moved as suspended load (Bennett et al., 1998). Subaqueous dunes are formed primarily through bedload processes. However, dunes can also form under mixed transport conditions, where a significant fraction of the bed material is able to be carried as suspended load and the suspended load may contribute to bedform migration once deposited (e.g., Kostaschuk et al., 2009; Naqshband et al., 2017).

2.2 Fluid and sediment composition

Application of terrestrial sediment transport formulae to other planetary bodies requires adjustment of a number of parameters, notably gravitational acceleration, fluid viscosity and the densities of fluid and sediment particles. Here we follow Burr et al. (2006) in the choice of parameters (Table 1). Similar to Earth, sediment transport on Mars involves the movement of particles of silicate material eroded from the planet's crusts. Sedimentary systems on Earth often host highly processed sediments that are chemically and mineralogically relatively mature, with abundant quartz and clay minerals. In contrast, Martian counterparts appear less mature hosting first-generation sediments, dominated by basaltic sedimentary rocks with only modest modification by liquid water (Deit et al., 2016). Immature sediments may be inferred to be a consequence of a lack of active plate tectonic processes on Mars (Cannon et al., 2015); although patterns of magnetization may suggest that Mars' crust formed by similar processes to that on Earth, during an early era of plate tectonics (Connerney, 1999; Connerney et al., 2005). Alternatively, immature sediments may be due to limited weathering on the surface of Mars, which only experienced transient periods of surface water (Ehlmann et al., 2011).

Titan's volatile cycle involves hydrocarbons that exchange between the surface, subsurface and a nitrogen-based atmosphere (Burr et al., 2013; Hayes et al., 2018). Both methane and ethane

cloud systems are recognised (Griffith et al., 2006). As considered here, surface flows forming fluvial features are thought to be composed of liquid methane that supply lakes and seas (Lunine et al., 1983; Ori et al., 1998; Burr et al., 2006; Hayes, 2016). Ethane is considered to be too involatile to be rapidly recycled by evaporation into Titan's atmosphere, restricting rainfall and runoff to methane cycling only (Lorenz and Lunine, 2005; Burr et al., 2006); although others have proposed surficial flows of both liquid methane and ethane (Hayes et al., 2018). Sediment on Titan is believed to occur as two compositional types: i) water-ice derived from Titan's outer crust and ii) organic material derived from the atmosphere through photochemical reactions of hydrocarbons (Imanaka et al., 2004; Burr et al., 2006; Schröder and Keller, 2008). There is significant uncertainty as to the density of organic particles and the exact types and proportions of liquid hydrocarbons (Burr et al., 2006; 2013). Densities of organic particles settling from the atmosphere on Titan could be as low as ~400 kg/m^3 (Bott, 1986). In this case, organic particles would be positively buoyant in surface liquid hydrocarbons assuming fluid densities of 450 kg/m^3 (Lorenz et al., 2003; Burr et al., 2006). However, for simplicity, only negatively buoyant particles are considered herein. The following analysis of sediment transport assumes noncohesive particles, applicable to systems lacking substantial amounts of clay on Earth and Mars. As discussed by Burr et al. (2013) for Titan sediments, this constraint may also be a reasonable assumption for water-ice particles, but may not be correct for sediments composed of, or covered by solid tholins.

2.3 Particle size range

A range of particle sizes occur on Earth, Mars and Titan that may be involved within fluvial sediment transport. The transport of silt to gravel grade material is considered in this work with a median particle size, $4 < d_{50} < 4000\ \mu m$. As shown later, this covers the broad range of sediment sizes which might be expected to be moved as suspended load, given reasonable estimates of flow depths and slopes. Images from the Huygens landing site on Titan showed rounded cobbles of 5-15 cm in

diameter sitting on a surface probably composed of finer-grained soft substrate (Tomasko et al., 2005; Lorenz et al., 2008). Large volumes of sand-size organic material occur in aeolian sand seas, which in the Xanadu area of Titan may be transported by transient rivers (Lorenze et al., 2006; Barnes et al., 2015). The atmosphere of Titan is also a probable source of finer, micron-sized 1-10 µm, organic aerosol particles (Waite et al., 2009; Barnes et al., 2015). On Mars, a similarly wide range in particle sizes are associated with ancient river systems. As mentioned, Rover data suggest fluvial deposits are composed of sandstones and gravels (Edgar et al., 2017). Also, observed are mudstones interpreted as lacustrine deposits with muds and silts potentially derived from rivers (Schieber et al., 2016).

The particle size distribution of sediment in natural environments is often wide and fine-tail skewed; this distribution being the motivation for the standard application of a log-normal particle size scale (Soulsby, 1997; Garcia, 2008). In the following work, polydisperse models with nonuniform particle sizes, use idealised sediment grain-size distributions, described by a natural ϕ-scale log-normal distribution (Middleton, 1970), where $\phi = -log_2(d/d_0)$, d is particle size in mm and d_0 is the standard grain diameter of 1 mm (Krumbein, 1934; Leeder, 1982). The particle size distribution is discretized into *N* size classes with a phi-scale bin size of 0.01. The log-normal distribution is truncated to include the central 99%, by removing the lowest and highest 0.5% of the probability distribution, to avoid overly small and large particles in the analysis.

3. Assessment of suspended-load-dominated flow

3.1 Sediment transport modes

Sediment moved by rivers and other turbulent shear flows display a continuum of transport behaviours, but is commonly considered in terms of two principle modes: particles transported as

"bed load", rolling, sliding or saltating in frequent contact with the bed (van Rijn, 1984a), and "suspended load", disperse through the flow, supported by turbulence (van Rijn, 1984b). Highlighting the continuous nature of sediment transport behaviour (Parsons et al., 2015), a "mixed load" category of transport is also defined for sediment which displays intermediate characteristics between bedload and suspended load (Dade & Friend, 1998; Church, 2006). It is also common to define the finest part of the suspended material – that does not form a significant component of the river bed, and the occurrence of which is governed by the upstream supply rate – as "wash load" (van Rijn, 1984a; Church, 2006). Because the analysis of equilibrium flow conditions in this work assumes all particles size classes are available for entrainment from the bed, a distinction between suspended load and wash load is not made.

3.2 Sediment transport thresholds

3.2.1 Incipient motion and entrainment

Whilst in this work we principally focus on suspended-load sediment transport, it is necessary for comparative purposes and computation of sediment entrainment rate (see below), to examine the threshold at which sediment on the bed begins to move, i.e., entrained as bedload, or for finer sediments as suspended load (Bagnold, 1966). The principal formulae for sediment transport criteria for the thresholds of motion, and suspension and equilibrium introduced later, are summarised in **Table 2**.

Shear from a flow imparts tangential and normal forces on solid boundaries including particles resting on the bed. The bed shear stress may be approximated using the standard momentum balance formula, which balances frictional and gravitational forces, assuming negligible downstream variation in flow (e.g., Parker et al., 2007),

$$\tau_* = g\rho hS. \quad (1)$$

where g, ρ, h and S are the acceleration due to gravity, fluid density and depth of the flow, and slope of the bed, respectively. The shear stress may also be characterized in units of velocity by the shear velocity, $u_* = (\tau_*/\rho)^{0.5}$, or in dimensionless form by the Shields number, that represents the ratio of fluid shear stress to the gravitational weight of a submerged particle (Shields, 1936), defined $\theta = \tau_*/g\Delta\rho d_{50}$, where $\Delta\rho = \rho_s - \rho$ is the particle-fluid density difference and d_{50} the median particle diameter. Importantly, because the Shields number takes into account the effects due to variable acceleration of gravity, particle and fluid density and grain size, it provides a suitable measure of the relative mobility (or intensity of sediment transport) of different planetary cases.

Above a critical shear stress applied to the bed, particles will be continuously transported. Where sediment density is constant, the critical Shields number, θ_{ci}, for incipient motion of $i = 1 \ldots N$ physically distinct classes of sediment, of diameter d_i, may be prescribed by the empirical formula proposed by Soulsby (1997),

$$\theta_{ci} = \frac{0.3}{1+1.2D_{si}} + 0.055(1 - e^{-0.02D_{si}}), \quad (2)$$

where the dimensionless particle diameter, $D_{si} = (g\Delta\rho/\rho\nu^2)^{\frac{1}{3}}d_i$ and ν is the fluid kinematic viscosity.

3.2.2 Sediment suspension

When the shear velocity has a similar or greater value than the particle settling velocity, $u_* \gtrsim w_{si}$, a substantial proportion of entrained particles may travel as suspended load within the flow supported

by fluid turbulence, with intermittent or limited contact with the bed (Rouse, 1937; Bagnold, 1966; Soulsby, 1997; Dade & Friend, 1998; Dorrell and Hogg, 2011). Here particle settling velocity, w_{si}, is prescribed by an empirical formula covering a combined viscous plus bluff-body drag law for natural irregular grains,

$$w_{si} = \frac{\upsilon}{d_i}\left[\left(10.36^2 + 1.049D_{si}^3\right)^{\frac{1}{2}} - 10.36\right]. \quad (3)$$

(Soulsby, 1997). Settling velocities for Earth, Mars and Titan based on Eq. (3), and using the particle properties in Table 1, are shown in **Figure 2**.

The distribution of suspended sediment in a shear flow is classically given by the Rouse profile, which assumes mixing throughout the total depth (Rouse, 1937). The concentration, $c_i(Z)$, of particulate material carried in suspension at a distance above the bed, $z = hZ$, where h is flow depth, is described by the Reynolds averaged mass conservation equation,

$$\frac{K}{h}\frac{\partial}{\partial Z}c_i(Z) + w_{si}c_i(Z) = 0. \quad (4)$$

Here the eddy diffusivity, K, describes diffusive mixing of sediment in suspension by turbulent fluid motion. The ratio of diffusive mixing momentum, the eddy viscosity ν_t, to diffusive mixing of sediment, eddy diffusivity, K, is described by the turbulent Schmidt number, $Sc_t = \nu_t/K$. For open channel flow, equating turbulent stress with eddy viscosity mixing from shear, the eddy viscosity is described by the function $\nu_t = \kappa u_* L f(Z)$, where the von Kármán's constant, $\kappa = 0.4$, u_* is the shear velocity, L is a mixing length and $f(Z)$ is a structure function describing the variation in turbulent mixing with depth. Also, it may be assumed that the mixing length $L = h$, the mixing length ratio

$\alpha = L/h \equiv 1$ (Dorrell & Hogg, 2012), and the structure function is parabolic $f(Z) = Z(1-Z)$ (Rouse, 1937). From these assumptions the Rouse profile for concentration, $c_i(Z)$, of each particle class is determined as

$$c_i(Z) = c_i^+ \left(\frac{Z^+}{1-Z^+}\frac{1-Z}{Z}\right)^{\beta_i}, \tag{5}$$

where c_i^+ is the sediment concentration, at a near-bed height Z^+, and

$$\beta_i = Sc_t w_{si}/\kappa u_* \tag{6}$$

is the Rouse number. Here the Schmidt number is taken as unity (Rouse, 1937). From Equation 5 a stratification shape function, λ_i, is determined that relates the depth-averaged concentration, c_i, to a near bed reference concentration, c_i^+,

$$\lambda_i = \int_{\frac{z^+}{h}}^1 \left(\frac{z^+}{h-z^+}\frac{1-Z}{Z}\right)^{\beta_i} dZ \text{ where } c_i \equiv \int_{\frac{z^+}{h}}^1 c_i(Z)\, dZ = \lambda_i c_i^+ \tag{7}$$

The total concentration of sediment in suspension at a height above the bed is thus, $c(Z) = \sum_{i=1}^{N} c_i(Z)$ and the depth-averaged concentration of sediment, $c = \int_0^1 c(Z)\,\mathrm{d}Z$.

In the literature, a range of values of the ratio of gravitational settling to turbulent dispersion,

$$B_i = w_{si}/u_*, \tag{8}$$

have been used to signify the threshold between bedload and suspended load transport ranging from $0.4 < B_i < 1.8$ (see discussions in Komar, 1980; Burr et al., 2006); reflecting the challenge of setting a distinct threshold on what is a transitional boundary or continuum of transport behaviour (Parsons et al., 2015). Bridge & Demicco (2008) considers that for values in the range of $1.2 < B_i < 1.5$, particles are moved upwards within a flow, and for $0.4 < B_i < 0.9$, particles remain in suspension due to turbulence. Others have concluded that $u_* = w_{si}$ defines an upper limit of the bed shear stress at which a concentration profile of suspended sediment starts to develop (van Rijn, 1984b; Niño et al., 2003). Based on Bagnold (1966), a value $B_i = 1.25$ has been generally used in previous analysis of planetary sediment transport (e.g. Komar, 1980; Burr et al., 2006; Grotzinger et al., 2013). The different values for B_i taken to signify the suspension threshold, may be a consequence of variations in the value of Sc_t (van Rijn, 1984b; Bennett et al., 1998; Cellino & Graf, 2002), but also due to the different definitions applied for estimating the threshold experimentally (Komar, 1980; Burr et al., 2006).

Using the Rouse equation, Dade & Friend (1998) examined the relationship between u_*/w_{si} and the fraction of the total sediment load carried as bedload,

$$\chi_b = (1 - \beta_i)/(\xi^{1-\beta_i} - \beta_i), \tag{9}$$

where the relative depth $\xi = h/z^+$, assuming the near-bed height z^+ and concentration, c_i^+, corresponds to the thickness and concentration, respectively, of the bedload layer. This approach elegantly shows how bedload versus suspended load fraction varies with w_{si}/u_*. From this analysis it may be seen that for $u_* = w_{si}$, the fractions of bedload and suspended load are approximately

equal, whilst for $w_s \ll u_*$, sediment is transported predominantly as suspended load (**Figure 3**). Dade & Friend (1998), applied the following criteria to distinguish load types for each particle class size: $w_{si}/u_* \leq 0.3$ for suspended load, $0.3 < w_{si}/u_* < 3$, for mixed load and $w_{si}/u_* \geq 3$ for bedload. It should be noted that the fraction of bedload, when B_i is small, is also a function of ξ. For the particle size ranges ($4 < d_{50} < 4000\,\mu m$) and flow depths ($1 < h < 10\,m$) considered in this work it is assumed that, $z^+ \ll h$, such that $\xi \gg 1$. This assumption is supported by models for the thickness of the bedload layer (e.g., Dorrell, 2010; Kumbhakar et al., 2018). For instance, the analysis of the highly concentrated collisional region at the base of sediment transporting flows, suggests $\xi > 10$, except in the case of shallow flows ($h/d < 2000$) with relatively high Froude numbers ($Fr > 0.5$) (see figure 5.10 of Dorrell, 2010).

3.4 Suspended-load-dominated transport field

To estimate the potential for suspended load, sediment transport regimes using the definitions defined by Dade & Friend (1998) are shown for different particle size versus the product of slope and depth, Sh (**Figure 4A**). Here w_{si} and u_* have been computed, as a function of d_{50} and Sh, for the different planetary cases (Table 1). It may be noticed from this plot that, firstly, there is only a relatively modest difference in regime boundaries for the different planetary cases (as noted in previous analysis of threshold boundaries e.g., Komar, 1980; Burr et al., 2006). Secondly, that sand grade and finer material will be transported dominantly in suspension at values of $Sh > 10^{-2}$. Lastly, that the bedload regime, as defined by the Shields criterion and $w_{si}/u_* = 3$, occupies a relatively small area of the Sh parameter space. Flow depths and slopes are poorly constrained for both Mars and Titan (Burr et al., 2013). Minimum and maximum estimates for Sh, as determined from flow depth and slope used in previous studies, Martian outwash channels (Komar, 1980; Wilson et al., 2004) and Titian channels (Perron et al., 2006), are shown and compared with those for Earth based on a global dataset (Dunne & Jerolmack, 2018) (**Figure 4B**). Assuming that the upper range in channel

Sh estimates are valid, this would suggest suspended-load-dominated systems may occur on both Mars and Titan for flows transporting sand, and even potentially gravel in the case of Martian outflow channels (as also surmised by Komar, 1980). Moreover, whilst the dynamics of coarser-grained systems may be expected to be dominated by bedload transport, these systems may also transport significant proportions of finer-grained material as suspended load or wash load, as observed for rivers on Earth (Turowski et al., 2010).

4. Assessment of equilibrium conditions

4.1 Equilibrium model

The suspension criterion outlined earlier, Eq. (8), describes the competence of a turbulent flow to support sediment in suspension as determined by its settling velocity. Critically it does not, however, provide a measure of whether a flow has the capacity to either support its existing sediment load, nor entrain further material, and thus whether a flow is erosional, depositional or in equilibrium under the imposed hydraulic conditions (Hiscott et al., 1994; Leeder, 2005; Dorrell et al., 2018). Here we apply the model developed by Dorrell et al. (2018), which introduces a Velikanov-Bagnold based flow power (Velikanov, 1954; Bagnold, 1966) entrainment model, to calculate the conditions for equilibrium flow. The equilibrium model, herein referred to as the "flow-power flux-balance" model, is based on a system of one-dimensional advection (settling) – diffusion (turbulence) equations, and uses an "active layer" of sediment at the top of the bed to exchange particles between the underlying bed and the overlying water column (i.e. flow), to describe the turbulent mixing and settling of suspended particles (Dorrell et al., 2013) (**Figure 5**). In this model, bedload transport processes are not explicitly modelled, although the active layer may be considered as a thin high-concentration bedload or "sheet flow" layer (Sumer, 1996). The model is thus strictly only applicable

to dilute flow where flow is vigorous enough to move sediment dominantly as suspended load and bedload becomes negligible (Dade & Friend, 1998; Dorrell, 2010; Dorrell et al., 2013). Under such conditions sediment can be directly entrained into suspension and the influence of bedload on the near-bed turbulence limited (Bagnold, 1966; Leeder et al., 2005; Niño et al., 2003). The limited role of bedload on controlling the overall dynamics of sediment transport for suspended-load regimes, $w_s/u_* < 1$, is also supported by the bankfull characteristics of rivers channels on Earth. Relatively fine-grained, suspended-load-dominated channels have bankfull steady-state regimes with substantially higher Shields numbers, compared to bedload channels that have values that approximate the threshold of motion (Dade & Friend, 1998). This observation suggests that the equilibrium state of suspended-load channels is dictated by the capacity of flows to suspended load under high-stage conditions, as opposed to bedload processes during high-stage or low-stage conditions (Dade & Friend, 1998).

Given an erodible substrate of loose sediment, flows entrain or deposit material to reach a balance between sediment entrainment and deposition. For suspended-load-dominated flow, equilibrium sediment transport is defined where the net rate of sediment entrainment from the bed equals the net rate of deposition from suspended load (Smith and Hopkins, 1973; Garcia and Parker, 1991, 1993; Garcia, 2008; Dorrell et al., 2013, 2018). For each particle class, sediment entrainment rate from the bed, E_i, is determined, after Dorrell et al. (2018), by

$$E_i = \varepsilon\rho(g\Delta\rho h)^{-1}\left(\max\left[u_*^2 - u_{*ci}^2, 0\right]\right)^{\frac{3}{2}}. \quad (10)$$

where ε=13.2 is an empirical parameter describing entrainment rate, based on a best fit to ten separate experimental datasets (Dorrell et al., 2018). Here Eq. (10) relates the work done lifting a

mass of sediment from the bed into suspension, in terms of available flow power above that needed for incipient motion.

The particle class dependent critical shear velocity, u_{*ci}, for incipient motion, from Eq. (2) is,

$$u_{*ci} = \sqrt{\frac{g\Delta\rho d_i \theta_{ci}}{\rho}}. \tag{11}$$

The deposition rate is given by the near-bed concentration of the suspension and particle settling velocity, $c_i^+ w_{si}$. Equilibrium flow is thus defined as satisfying

$$\frac{c_i^-}{c_m} E_i = c_i^+ w_{si} \forall_i , \tag{12a}$$

$$\sum_{i=1}^{N} c_i^- = c_m, \tag{12b}$$

describing the balance of deposition and erosion for all distinct particle classes ($\forall_i$) in suspension, Eq. (12a), and by the composition of the bed, Eq. (12b), see further Dorrell et al. (2013). In Eq. (12), for each independent particle class, the near-bed concentration of suspended sediment freely exchanged with the bed is denoted by c_i^+, defined at a height $z^+ = 0.01h$ above the bed (Soulsby, 1997) and the concentration of particles in the active layer, at the top of the bed that freely exchanges material with the flow, is denoted c_i^-. The near-bed concentration may be related to the suspended capacity of a given particle class by using a Rousean shape function, λ_i, describing the distribution of material in suspension, $c_i^+ = c_i/\lambda_i$, where c_i is the concentration for a particle class. Finally, a constant packing concentration in the bed, $c_m = 0.6$, is assumed (Dorrell and Hogg, 2010).

Equations (1)-(7) and (10)-(12) may be manipulated to yield the expression for the capacity of a given particle class,

$$c_i = \varepsilon \frac{\mathrm{c_i^-}}{\mathrm{c_m}} \frac{\lambda_i}{\mathrm{w_{si}}} \sqrt{\frac{g\Delta\rho h}{\rho}} \left(\frac{\rho}{\Delta\rho}\right)^{\frac{3}{2}} \left(S - \frac{u_{*ci}^2}{gh}\right)^{\frac{3}{2}}. \quad (13)$$

As particle concentration is dependent on the concentration of the active layer, $\mathrm{c_i^-}$, the relationship between bulk flow-capacity and slope (or shear stress) is not unique. However, equilibrium slope, at fixed capacity, has a weak non-linear dependence on reduced gravity of suspended sediment, $g\Delta\rho/\rho$, scaling to a power of one third, and a stronger linear dependence on fluid density. This outcome being a consequence of settling velocity scaling with reduced gravity and in well-mixed suspensions $\lambda_i \sim 1$ (Dorrell et al., 2013). Critically, the leading order relationship between flow capacity, Eq. (13), recovers observations first made by Gilbert and Murphy (1914), where flow concentration was related to slope via:

$$c \equiv \sum_{i=1}^{N} c_i \propto (S - S_c)^{\frac{3}{2}}, \quad (14)$$

where S_c denotes the slope required for incipient motion, called the "competent slope" by Gilbert and Murphy (1914). Here, the flow-power based entrainment model (Dorrell et al., 2018) is, for the first time, shown to unify the Gilbert and Murphy (1914) capacity model with Shields (1936) criterion for initiation of motion, with a slope of competence $S_c = u_{*ci}^2/gh$.

The flow-power, flux-balance model described here, is valid for open channel flows, carrying relatively low concentrations of noncohesive material, where sediments are predominately transported by turbulent fluid motion as suspended load, and the mass of sediment supported by

particle-particle and particle-bed interactions is negligible (Dorrell et al., 2013). It also assumes that all particle size classes occur within the bed and are not limited to the flow by supply from the bed: as such the results are applicable to transport (capacity) limited alluvial channels but not necessarily supply limited channels. The polydisperse form of the equilibrium model, as applied here, takes into account particle size distribution effects, that have a marked influence on the equilibrium condition (McLean, 1992; Dorrell et al., 2013; 2018). It should be noted that an inherent uncertainty within our and previous similar analyses is the application of constants, based on Earth-derived data, including those constants for instance used in Eqs. (2 & 10): investigation of sediment transport under different gravitational conditions (e.g., Kleinhans et al., 2011), would be required to understand their dependency on gravity.

4.2 Equilibrium shear stress

An evaluation of the dimensional shear stress at equilibrium for different median grain sizes and particle size standard deviations is shown for Earth (**Figure 6A**) and for different planetary bodies (**Figure 6B**). These results are for a single case of flow depth, $h = 1\,\mathrm{m}$, and sediment concentration, $c = 0.1\%$, or $0.001\,\mathrm{v/v}$ (sediment volume per total volume), within the range for rivers on Earth: noting that depth and sediment concentration values vary substantially for rivers on Earth (e.g., van Maren et al., 2009) and probably also on other planetary bodies (see discussion in Kleinhans 2005; Burr et al., 2006; Hoke et al., 2014). For comparison the criteria for the initiation of motion ($u_* = u_{*c}$) and onset of suspension ($w_s = u_*$) are also shown. Predicted equilibrium shear stresses are several times lower on Mars, and more than ten times lower on Titan, in comparison with Earth (**Figure 6B**). The results also show, for all planetary cases, that: i) the equilibrium shear stress condition takes a different form, and has substantially higher values, than the Rouse criterion for suspension ($u_* = w_s$) and; ii) higher shear stresses are required to maintain equilibrium for flows carrying coarser and more poorly-sorted material in suspension (see also Dorrell et al., 2018).

In order to better understand the effects of gravity and particle-fluid properties, it is also instructive to plot shear stress with the acceleration due to gravity, here shown for a single particle size for each of the particle-fluid cases (**Figure 7A**). The formulae in **Table 2** have been used to compute the shear stress that satisfy equilibrium and the threshold of motion and suspension criterion ($u_* = w_s$). This analysis shows that the shear stress required for all sediment transport criteria scales positively with gravity. Increasing shear with increasing gravity is a necessary consequence of increased work done keeping sediment in suspension (Bagnold, 1966). In addition, gravity also influences the vertical distribution, i.e. stratification, of material in suspension as described by λ_i (Eq. (7)) as a function of the Rouse number, β_i (Eq. (6)). Because particle settling velocity, w_s, increases linearly with gravity, whilst shear stress varies with gravity, as $u_* = \sqrt{ghS}$, it follows that the particle stratification becomes stronger (i.e. less evenly distributed through the flow depth) with gravity, increasing proportional to the square root of gravity. Therefore, on Mars and Titan particles of a given size require less dimensional force to be transported; or alternatively, for a given shear stress larger grains will be moved compared with Earth.

4.3 Dimensionless shear stress

The results for shear stress are replotted in **Figure 6C-D** in terms of the Shields parameter. The Shields parameter normalises for gravity, as well as the difference in fluid and particle densities, and hence provides a more appropriate estimate of the relative mobility of sediment transport for different planetary cases. Here we see there is limited variation between the dimensionless shear stress at equilibrium flow between different planetary cases with different particle-fluid systems (Table 1). Moreover, it is apparent from **Figure 6C-D** that the standard deviation of the suspended load particle size distribution exerts a prime control on equilibrium flow conditions, comparable if not larger than that exerted by the median grain size.

The variation in dimensionless criteria for incipient motion, suspension and equilibrium flow with gravity indicates that the various forces acting on particles are not affected in equal measure (**Figure 7B**): resulting in a change in the critical Shields values of these criteria for a particular particle size. The Shields number for incipient motion decreases with dimensionless particle size, $D_s = (g\Delta\rho/\rho\nu^2)^{\frac{1}{3}}d$ (Soulsby, 1997) and thus it also decreases proportional to increasing gravity (**Figure 7B**), even though dimensional shear stress for incipient motion increases with gravity (**Figure 7A**). The criteria for suspended-load-dominated flow and equilibrium flow both increase proportional to gravity. For a particular particle-fluid case, the variation in Shields numbers, over the range of planetary gravities considered is relatively modest, changing by less than an order of magnitude. Due to the different particle and fluid properties for different planets, the difference in Shields values between planetary cases at their respective values of gravity, is smaller compared with any single particle-fluid case. Hence, the fundamental force balance ratios that control sediment transport are similar for the different planetary cases, with Earth having slightly higher Shields number values compared with Mars and Titan for the case of water-ice particles, and similar values to Titan for the case of organic particles.

4.4 Equilibrium slope

Flow conditions can be translated to equilibrium channel slope or slope-depth product, using the standard momentum balance formula, which balances frictional and gravitational forces, assuming negligible downstream variation in flow (Eq.(1)). Equilibrium slopes are thus directly related to the equilibrium shear stress, but scaled with flow depth instead of reduced density and median particle diameter, as per the dimensionless Shields number. Considering the same suspended-load concentration and flow depth as before, equilibrium slope is shown for variable particle size and particle size distributions (**Figure 8A-B)**. Note the slope gradient has an inverse proportional relationship with depth, where lower slopes are required to maintain equilibrium conditions for

deeper flows (Eq.(1)). Both particle size and size distribution have a strong effect on the equilibrium slope, with increased slopes required to carry sediment of a larger size and wider particle size distribution. This result is dictated by the requirement for increased shear velocities for coarser grained and more poorly sorted mixtures (**Figure 6A-B**).

The results show that the difference between predicted equilibrium slopes for planetary bodies are modest, suggesting a relatively weak dependency on gravity. This supposition may also be shown by plotting equilibrium slope with gravity for a single particle size for each of the particle-fluid cases (**Figure 9A**). For any particle-fluid case there is a decrease of equilibrium slope with decreasing gravity. For equilibrium flow, $u_s \propto \sqrt{g}$, the slope-gravity dependence is the result of the weaker scaling of entrainment with gravity than that of settling velocity,

$$E \propto \frac{u_s^3}{g} \propto g^{\frac{1}{2}}, \tag{15}$$

$$w_s \propto g. \tag{16}$$

The weaker scaling of entrainment is due to the balance between increasing available flow power and work done lifting sediment into suspension (Dorrell et al. 2018). However, the particular planetary particle-fluid properties of the cases considered interact to limit the differences, between Earth and the other planets, to within about a factor of two. The net result of gravity and particle-fluid effects is that silica-water systems on Earth are predicted to have steeper equilibrium slopes than basaltic-water systems on Mars and water-ice methane systems on Titan. Whereas, owing to the larger particle density, organic-rich transport systems on Titan are predicted to have steeper slopes than their water-ice counterparts on Titan and silica systems on Earth.

4.5 Equilibrium discharge

Following the approach taken by Burr et al. (2006), unit discharge ($m^2\ s^{-1}$) is approximated by

$$Q = uh = \frac{u_*^3 \sqrt{\frac{8}{f_c}}}{gS}\ , \tag{17}$$

where u is the depth-averaged velocity, and the Darcy-Weisbach formula for a sand bed,

$$\sqrt{\frac{8}{f_c}} = 8.16\left(\frac{R}{D_{50}}\right)^{0.1005}\ , \tag{18}$$

where R is the hydraulic radius, which for natural broad terrestrial channels can be approximated by the channel depth, and f_c is a non-dimensional frictional coefficient determined from Eq. (18) (for full discussion of this approach, see Burr et al., 2006); noting the use of Earth-based empirical constants within this formulation. From Eq. (17), discharge at equilibrium conditions may be estimated, and similar to shear stress and slope, shows a dependency on suspended-load particle size and particle size distribution (**Figure 8C-D**). Predicted discharges vary proportionally with gravity, such that lower discharges should be expected in reduced gravity environments for the same flow depth, concentration and particle size distribution (**Figure 9B**).

Given the uncertainty in respect of the selection of appropriate values for grain size and flow parameters on Mars and Titan, especially in the case of Martian palaeo-channels, estimating discharge is inherently problematic. Thus, here we show a probabilistic assessment of equilibrium discharge based on 2000 evaluations, using a uniform sampling of a range of flow depths ($1 < h <$

$10\,m$), median particle sizes ($-2 < \phi < 4$) and particle size distributions ($0.01 < \sigma < 2$) (**Figure 10A**). Particle concentration has not been varied here but is an additional controlling parameter on equilibrium flow shear stress and therefore discharge rate. The corresponding probabilities for equilibrium slopes are also shown (**Figure 10B**). These results are within the range of previous estimations based on hydraulic geometry i.e. relationships between discharge and channel dimensions (e.g., Lorenz et al. 2008; Burr et al., 2010; Konsoer et al., 2018). For comparison, the same probability analysis has been conducted applying the criteria for the threshold of suspension, $u_* = w_s$ (**Figure 10C-D**) and motion, $u_* = u_{*ci}$ (**Figure 10E-F**). These thresholds have been used to predict minimum discharges (e.g., Burr et al. 2006) and provide values substantially lower than those calculated for equilibrium flow conditions. For channels on Titan, discharge rates may be better constrained using slope values derived from stream profiles (Dhingra et al. 2018). The Hubur and Saraswati channels have average slope gradients of 1.1 x 10^{-3} m/m (see Supplementary **Figure S1**). Discharge estimates based on slopes ± 50% of this slope value suggest median P50 unit discharge rates of ~10 m^2/s for these channels for equilibrium flow conditions (**Figure 10A**).

5. Discussion

In the discussion, we summarise and discuss the key findings of our results. Here we focus on four themes: sediment transport under reduced gravity (section 5.1), implications for the depositional record (section 5.2), equilibrium slope and the use of submarine channels as analogues (section 5.3), and implications for predicting discharge (section 5.4).

5.1 Sediment transport under reduced gravity

Sediment transport formulae have been applied previously to constrain flow conditions (e.g., flow depth, velocity, unit discharge and shear stress) required to entrain and transport sediment by

surficial flow under reduced gravity on Mars and Titan (e.g., Miller & Komar, 1977; Komar, 1979; 1980; Burr et al., 2006; 2013; Grotzinger et al. 2013; McSween et al., 2019). In this work, we have focussed on the conditions required for particle suspension, specifically suspension-dominated flow (**Figure 4**) and conditions for equilibrium flow by application of a new suspended-load equilibrium model (**Figures 6-9**). As outlined below, the results presented here build on previous work where the threshold values for initial motion use Shields (1936) approach, transport is based on the Rouse (1937) model of sediment suspension, and a new flux boundary condition (Dorrell et al., 2018) is employed to close the model for suspended-load equilibrium flow.

Whilst sediment can be viewed to move more "easily" in reduced gravity environments, given the lower dimensional shear stress values (or shear velocity) required for particle motion and suspension (Miller & Komar, 1977; Komar, 1980; Burr et al., 2006; Grotzinger et al. 2013; McSween et al., 2019), the impact of gravity on sediment transport is not straight-forward, having opposing effects on the particle settling velocity and fluid flow (Miller and Komar, 1977; Komar, 1980). The combined effect of gravity results in an overall modest, albeit still potentially significant, variation in the ability of flows to transport sediment under different gravity conditions: as best illustrated by the critical Shields numbers (**Figures 6A-B & 7B**) and slope-depth product (**Figure 8A-B & 9A**) required for sediment-transport thresholds and equilibrium conditions. From our analysis it can be seen that variations between the planetary cases considered (Table 1) are reduced, compared with that of a single particle-fluid case, by the effect of fluid-particle properties.

To distinguish sediment transport modes, previous work has often applied the condition $B = 1.25$ for the onset of particle suspension (Komar, 1980; Burr et al., 2006). Following Dade & Friends (1998), here we have taken $B = 0.3$ to instead signify suspension dominate flow (**Figure 3**), and assessed equilibrium suspended flow based on a flux-balance model. Whilst both these approaches show that higher shear stresses are necessary for suspended-load-dominated flow, compared with $B = 1.25$ (**Figure 4A & Fig. 6**), they similarly indicate that sediment should be readily

carried in suspension on Mars and Titan. This supposition, however, assumes the availability of sufficiently fine-grained material and similar bankfull slope-depth products as observed on Earth (**Figure 4A**). Environments with a reduced gravity require lower dimensionless shear stresses and values of slope (or slope-depth product) for suspended-load sediment transport. Thus, there exists a marginally higher potential for suspended-load-dominated flows on Mars and Titan compared with Earth (**Figure 4, 6D & 7B**) (as noted previously by Komar (1980) and Burr and Parker (2006)). Interestingly, this contrasts with current satellite and surface based observations of fluvial systems on Mars, the depositional characteristics of which overwhelmingly are interpreted to reflect bedload-dominated transport regimes (e.g., Wood, 2006; Williams et al., 2013; Dietrich et al. 2017; Edgar et al., 2017). These observations may reflect a physical bias towards bedload transport on these planets, for instance, due to the flow conditions and available sediment size. Alternatively, it may reflect an observational bias towards coarse-grained bedload deposits, that are better preserved in outcrop and more easily observed than finer-grained deposits of suspended-load-dominated systems.

The higher propensity for suspended-load-dominated flow, however, does not necessarily hold for cases of high-density fluid-particles ratios, as may apply to organic particles on Titan (**Figure 7B**) nor for coarser particles sizes (>~1 mm) on Mars (**Figure 4**). Furthermore, Shields numbers and slope-depth values required for initial motion increase under reduced gravity conditions (**Figure 7B & 9A**) making bedload transport effectively "harder" on Mars and Titan compared with Earth.

Critically the results show that substantially higher shear stresses, and thus also Shields numbers and values of slope-depth product, are required to satisfy the equilibrium condition compared with the commonly applied suspension criterion, $B \cong 1$, on Earth and other planetary bodies (see also Dorrell et al., 2018); with ramifications for predicted slope and discharge of suspended-load-dominated systems. Moreover, equilibrium conditions are governed strongly by the particle size distribution carried or available to flows, with significant implications for the

applicability of monodisperse sediment transport models, that use a single characteristic particle size (e.g., McLean, 1992; Dorrell et al., 2013, Dorrell et al., 2018). In terms of sediment transport analysis, particle size distribution provides an additional source of uncertainty, especially because quantification of appropriate size distributions of suspended sediment is challenging, and even more so for extra-terrestrial systems. The results presented for equilibrium flow are valid for alluvial channels where suspension dominates the transport process and flow is not supply limited by an armoured bed or other limitations on the availability of sediment. It should also be noted that cohesive effects are not modelled, which are clearly important in many terrestrial systems, and potentially apply to Martian palaeo-channels (Matsubara et al., 2015; Lapôtre et al., 2019). Alternative models, or modification to the current model, would be required to explicitly explore channel dynamics beyond the scope of the current model (e.g., bedload-dominated, bedrock, supply-limited and cohesive channels).

5.2 Implications for the depositional record

Whilst modest differences exist in terms of transport potential between planetary cases, these differences may affect the character of sedimentary systems. Given the same slope and flow depth, and with the exception of high fluid-particle ratio systems, somewhat coarser sand – by up to ~100 μm – may be moved in suspension on Mars and Titan compared with Earth (**Figure 8B**). This material may also be moved further leading to overall longer transport systems (Burr and Parker, 2006). Hence, under reduced gravity conditions a higher fraction of coarse sediment load may be expected to be transported by rivers and streams, which would impact the characteristics of fluvial and other sedimentary systems. For instance, shoreline systems and submarine-fan systems fed by sediment derived from rivers should be overall coarser-grained compared with their terrestrial counterparts. In terms of bedforms, the regime boundary bedforms formed principally under bedload and suspended-load-dominated flow (i.e. between ripples/dunes and transitional/upper plane bed

conditions) should be shifted to coarser particle sizes for grain sizes in the range of 100-500 μm (a subtle effect also indicated within previously published bedform stability diagrams e.g., see figure 10c of Grotzinger et al, 2013). Moreover, given the greater propensity for suspended-load-dominated load flow under reduced gravity, bedforms produced under transitional and upper plane bed regimes may be overall more prevalent than those associated with bedload during lower regime flows (i.e. ripple and dune regimes). The greater prevalence of material to be transported as suspended-load (and wash load) under reduced gravity, has also been speculated to be a possible reason for the rarity of alluvial depositional landforms on Mars (Burr & Parker, 2006; Carling et al., 2009). The variations in sedimentary systems discussed above would be expected to be reversed in the case of high-density organic particles on Titan.

5.3 Equilibrium slope and submarine channels analogues

Results indicate that under reduced gravity conditions alluvial geomorphological forms developed by suspended-load flows should tend towards gentler slopes compared with equivalent systems on Earth (**Figure 8B & 9A**); here again excepting high fluid-particle ratio systems. This outcome is in contrast to other recent work that has concluded channels should adjust to become steeper under reduced gravity conditions. This alternate conclusion is based on the analysis of terrestrial hydraulic geometry data (i.e. relationship between bankfull channel geometry and discharge), specifically the relationship between channel geometry and unit driving-force for fluvial and submarine channels (Konsoer et al., 2018). Here we explain the rationale proposed for using submarine channels as analogues for extra-terrestrial channels developed under reduced gravity, and why submarine channels should be expected to develop steeper slopes compared with rivers, before examining if the conclusion that steeper channels should form on planets with a reduced gravity is valid.

Submarine channels formed by turbidity currents on Earth have been used as analogous for subaerial river and outwash channels formed under reduced gravity (Komar, 1979; Konsoer et al.,

2018). This approach is based on the reasoning that, due to the buoyancy created by the ambient water, the "effective gravity" acting on a turbidity current is reduced. For a turbidity current, the shear velocity may be approximated by $u_* = \sqrt{g'hS}$, where the "reduced gravity", referred to as the "current's reduced gravity" to distinguish it from planetary gravity, $g' = g(\rho_{c-}\rho_a)/\rho_a$, and ρ_c and ρ_a are the densities of the current and the ambient fluid, respectively (Kneller & Buckee, 2000; Kneller, 2003). Konsoer et al. (2018) presented data showing that submarine channels have slopes up to three orders of magnitude steeper than their fluvial counterparts of comparative bankfull hydraulic geometry. They thus concluded that channels formed under reduced gravity on other planets also should adjust to steeper quasi-equilibrium slopes.

Recalling Eq. (1), for open channel flows, the slope at equilibrium conditions should satisfy, $S = \tau_{*e}/\rho gh$. For turbidity currents, channel slope similarly should follow, $S = \tau_{*e}/\rho g'h$. Given values appropriate for Earth ($g = 9.8$ ms^{-2}, $\rho_a = 998$ kgm^{-3}, $\rho_s = 2650$ kgm^{-3} and assuming $0.01 < c(\%) < 1$), values for the current's reduced gravity range between $0.002 < g' < 0.2$. By virtue of the fact that, $g' \ll g$, and the shear stress required for equilibrium, τ_{*e}, does not vary substantially between open channel flows and turbidity currents, it may be seen that turbidity currents require at least an order of magnitude higher slope, than those for rivers, to maintain equilibrium conditions. The increased slope of submarine channels compared with river systems (as observed by Konsoer et al., 2013; 2018), can therefore be understood to be a consequence of the reduced shear stress imposed by turbidity currents on the bed, as a function of g'.

Turbidity currents on Earth, like rivers under reduced gravity environments on smaller planetary bodies, impose a smaller shear stress on the bed compared with terrestrial rivers (**Figure 7A**). However, turbidity currents cannot directly replicate geophysical flows on other planets due to the gravity term, which describes particle dynamics (Eqs. (15 & 16)), being different when comparing Earth and other planets.

5.4 Implications for the discharge predictions

Constraining the discharge of channels on Mars and Titan is of particular interest given that predicted values may be used to evaluate precipitation rate and hence climate (Perron et al., 2006; Lorenz et al., 2008), or on Mars, outflows of subterranean water (Carr, 1979; Baker, 2001). Minimum discharge predictions have been made previously based on a "threshold channel approach", by calculating the shear velocity required to entrain and transport sediment using the critical Shields number for channel bed sediment (e.g., Burr et al., 2006; Perron et al., 2006; Dietrich et al. 2017; Morgan & Craddock, 2019). This method assumes bedload-dominated transport in channels, which whilst it may be appropriate for gravel-bed channels, may not be valid for finer-grained channels (**Figure 4**; Dade and Friend, 1998; Church, 2006). If suspended load conditions instead are assumed to dominate, application of a capacity criterion for suspended load, such as that provided by the equilibrium model used here, to estimate bankfull flow conditions leads to substantially higher predictions of discharge (**Figure 10**). Moreover, it should be noted that equilibrium conditions, as predicted by the flux-balance approach, yields results that differ in contrast to the application of the Rouse suspension criterion. Given the large uncertainties in the channel boundary conditions of extra-terrestrial channels, a probability-based analysis may be more appropriate for estimating probable channel discharges (Figure 10).

Alternatively, given the limited availability of grain size and other required boundary conditions, hydraulic geometry relations have been used to estimate channel discharge (Dietrich et al., 2017; Morgan & Craddock, 2019). A gravity correction commonly is applied using gravitational scaling factors (e.g., Irwin et al., 2005; Burr et al., 2010), however, based on the analysis of submarine channels this was considered unnecessary (Konsoer et al., 2018). As discussed in the previous section, it may be concluded that sediment transport in submarine channels do not represent faithfully the physics of sediment transport under reduced gravity conditions. Using the equilibrium model it can be shown that discharge varies with gravity for flows of the same depth

(**Figure 9B**). Channels developed under different strengths of gravity, therefore, do not follow a unique hydraulic geometry discharge-depth relationship (**Figure 11**). Thus, this result suggests scaling factors should be applied to terrestrial hydraulic geometry data in order to correct for the effect of gravity.

6. Summary

In this work constraints for suspended-load transport on different planetary bodies have been examined applying a theoretical model for equilibrium sediment transport (zero net erosion and deposition). The equilibrium model presented is applicable to transport (capacity) limited alluvial channels and, for the first time, unifies the Gilbert relationship for slope and flow capacity with the Shields criterion for incipient motion. The hydraulic modelling results presented here suggest the following key findings:

1. Substantially higher shear stresses, Shields numbers and slope-depth values, are required for suspended-load equilibrium sediment transport compared with values predicted by the commonly used suspension criterion ($w_s \cong u_*$). Moreover, the equilibrium condition is strongly governed by the suspended particle size distribution of flows, highlighting the limitation of monodisperse models to accurately forecast sediment transport parameters (McLean, 1992; Dorrell et al., 2013, Dorrell et al., 2018).
2. Only modest differences exist in a flow's ability, as assessed using the Shields parameter or slope-depth product, to transport sediment on Earth, Mars and Titan. This conclusion mainly is due to the compensating effects of gravity on sediment transport, that influences both the bed shear stress and particle settling velocity, but also the physical properties of the dominant particle-fluids systems, that partially compensates for differences produced by gravity. This work thus agrees with the synopsis of Komar (1980).

3. Suspended-load-dominated flow should be achievable on Mars and Titan, assuming the availability of sufficiently fine-grained sediment and flow depths and channel slopes comparable to those on Earth. With the exception of systems involving high particle-fluid density ratios, such as may apply to organic particles on Titan, there should exist a slightly higher propensity for suspended-load-dominated regimes in reduced gravity environments compared with Earth.
4. Making the assumption that Martian or Titanian channels were formed by suspended-load-dominated flows, leads to the prediction of substantially higher discharges for channels, compared with mechanistic-based models for bedload channels. Application of the equilibrium model, also provides higher discharge prediction than the suspension criterion $w_s \cong u_*$. This outcome has significant implications for precipitation models, and would indicate relatively high discharges due to wetter climates or larger outwash flood events.
5. Suspended-load channels at equilibrium should develop gentler slopes under reduced gravity conditions. This conclusion is opposite to the notion that channels morphologically adjust to steeper slopes under a reduced gravity, as has been proposed previously based on generalized hydraulic geometry relationships of submarine channels. We suggest that the use of submarine channels as analogues for extra-terrestrial river channels formed under a reduced gravity compared with Earth is flawed. This conclusion is because the net effect on sediment transport of a reduced planetary gravity, g, is not the same as that caused by a turbidity current's "reduced gravity", g'.
6. Overall, the modest variations of the transport ability of flows and equilibrium slopes on different planets, suggests that planetary surfaces should evolve self-similar fluvial forms. However, it may be speculated that the relatively small variations that do exist between planets could still result in variations in the character of sedimentary systems on different planets and the depositional record.

Acknowledgments

We thank editor Rosaly Lopes, Paul Carling and an anonymous reviewer for their comments that helped to significantly improved the paper and Devon Burr for helpful discussion. RMD thanks NERC for funding NE/S014535/1. The Turbidites Research Group of the University of Leeds, and their sponsoring companies, are also recognised for their support of earlier associated work.

Notation

β Rouse number

θ Shields number

θ_c Critical Shields number for incipient motion

θ_s Critical Shields number for suspension

θ_e Critical Shields number for equilibrium

κ von Kármán constant

λ Stratification shape function for particle concentration

μ Dynamic viscosity

ν Kinematic viscosity

ν_t Eddy viscosity

ρ, ρ_s Fluid and particle density

$\Delta\rho$ Difference in particle and fluid density

ρ_c, ρ_a Current and ambient fluid density for a turbidity current

τ_* Bed shear stress

τ_c Critical shear stress for incipient motion

τ_s Critical shear stress for suspension

τ_e Critical shear stress for equilibrium

B the ratio of particle setting velocity to shear velocity, w_{si}/u_*

c_i Individual particle class concentration

c Total particle class concentration at equilibrium (i.e. capacity)

c_m Packing concentration of the bed

c_i^+ Particle class concentration of suspended sediment at height z^+ above the bed

c_i^- Particle class concentration in the active layer at the top of the bed

d_i Particle diameter of the *i*th particle class

d_{50} Median particle diameter

D_s Dimensionless particle diameter

E_i Entrainment rate from the bed of the *i*th particle class

f_c Dimensionless frictional coefficient in the Darcy-Weisbach formula

g Gravitational acceleration

g' Reduced gravitational acceleration (turbidity current)

h Flow depth

i Index parameter indicating the *i*th particle class

K Eddy diffusivity

L Mixing length

Q Unit discharge

r Submerged specific density of a particle, $r = \Delta\rho/\rho$.

R Hydraulic radius of a channel

S Slope of the bed (m/m)

S_c Slope of competence

Sc_t Turbulent Schmidt number

u Depth-averaged flow velocity

u_* Shear velocity

u_{*c} Critical shear velocity at incipient motion

u_{*e} Critical shear velocity for equilibrium

w_s Particle settling velocity

z Height above the bed

z^+ Reference height above the bed

Z Dimensionless height above the bed

Declaration of interests

☒ The authors declare that they have no known competing financial interests or personal relationships that could have appeared to influence the work reported in this paper.

References

Achille, G.D., Hynek, B.M., 2010. Ancient ocean on Mars supported by global distribution of deltas and valleys. Nature Geoscience 3, 459–463. doi:10.1038/ngeo891

Andrews-Hanna, J.C., Lewis, K.W., 2011. Early Mars hydrology: 2. Hydrological evolution in the Noachian and Hesperian epochs. Journal of Geophysical Research 116. doi:10.1029/2010je003709

Bagnold, R.A., 1966. An approach to the sediment transport problem from general physics. U.S. Geological Survey Professional Paper 422-I, U.S. Government Printing Office, Washington, D.C. doi:10.3133/pp422i

Baker, V.R., Strom, R.G., Gulick, V.C., Kargel, J.S., Komatsu, G., Kale, V.S., 1991. Ancient oceans, ice sheets and the hydrological cycle on Mars. Nature 352, 589–594. doi:10.1038/352589a0

Barnes, J. W., Lorenz, R.D., Radebaugh, J., Hayes, A. G., Arnold, K., Chandler, C., 2015. Production and global transport of Titan's sand particles. Planetary Science, 4:1, doi: 10.1186/s13535-015-0004-y

Bennett, S. J., Bridge, J. S., & Best, J. L., 1998. Fluid and sediment dynamics of upper stage plane beds. Journal of Geophysical Research: Oceans, 103(C1), 1239-1274. doi:10.1029/97jc02764

Bott, D., 1986. Structural basis for semiconducting and metallic polymers. In: Skotheim, T. (Ed.), Handbook of Conducting Polymers, vol. 2. Dekker, New York, pp. 1191–1232.

Burr, D. M. and Parker, A. H., 2006. Grjot´a Valles and implications for flood sediment deposition on Mars. Geophysical Research Letters, 33, L22201, doi:10.1029/2006GL028011.

Burr, D., Emery, J., Lorenz, R., Collins, G., Carling, P., 2006. Sediment transport by liquid surficial flow: Application to Titan. Icarus 181, 235–242. doi:10.1016/j.icarus.2005.11.012

Baker, V. R., 2001. Water and the Martian landscape. Nature, 412, 228–236.

Burr, D.M., Williams, R.M.E., Wendell, K.D., Chojnacki, M., Emery, J.P., 2010. Inverted fluvial features in the Aeolis/Zephyria Plana region, Mars: Formation mechanism and initial paleodischarge estimates. Journal of Geophysical Research 115. doi:10.1029/2009je003496

Burr, D.M., Perron, J.T., Lamb, M.P., Irwin, R.P., Collins, G.C., Howard, A.D., Sklar, L.S., Moore, J.M., Ádámkovics, M., Baker, V.R., Drummond, S.A., Black, B.A., 2013. Fluvial features on Titan: Insights from morphology and modeling. Geological Society of America Bulletin 125, 299–321. doi:10.1130/b30612.1

Cardenas, B.T., Mohrig, D., Goudge, T.A., 2017. Fluvial stratigraphy of valley fills at Aeolis Dorsa, Mars: Evidence for base-level fluctuations controlled by a downstream water body. GSA Bulletin 130, 484–498. doi:10.1130/b31567.1

Carling, P., Burr, D., Johnsen, T., & Brennand, T., 2009. A review of open-channel megaflood depositional landforms on Earth and Mars. In D. Burr, P. Carling, & V. Baker (Eds.), Megaflooding on Earth and Mars (pp. 33-49). Cambridge: Cambridge University Press. doi:10.1017/CBO9780511635632.003

Cannon, K.M., Mustard, J.F., Salvatore, M.R., 2015. Alteration of immature sedimentary rocks on Earth and Mars: Recording aqueous and surface–atmosphere processes. Earth and Planetary Science Letters 417, 78–86. doi:10.1016/j.epsl.2015.02.017

Carr, M. H., 1979. Formation of Martian flood features by release of water from confined aquifers. Journal of Geophysical Research, 84, 2995–3007.

Carr, M. H., 2012. The fluvial history of Mars. Philosophical Transactions: Mathematical, Physical and Engineering Sciences, 370, 2193-2215.

Church, M., 2006. Bed Material Transport and the Morphology of Alluvial River Channels. Annu. Rev. Earth Planet. Sci., 34, 325–354. doi: 10.1146/annurev.earth.33.092203.122721

Collins, G.C., 2005. Relative rates of fluvial bedrock incision on Titan and Earth. Geophysical Research Letters, 32, L22202, doi:10.1029/2005GL024551

Connerney, J.E., 1999. Magnetic Lineations in the Ancient Crust of Mars. Science 284, 794–798. doi:10.1126/science.284.5415.794

Connerney, J.E.P., Acuna, M.H., Ness, N.F., Kletetschka, G., Mitchell, D.L., Lin, R.P., Reme, H., 2005. Tectonic implications of Mars crustal magnetism. Proceedings of the National Academy of Sciences 102, 14970–14975. doi:10.1073/pnas.0507469102

Dade, W. B. & Friend, P. F., 1988. Grain-size, sediment - Transport Regime, and channel slope in alluvial rivers: The Journal of Geology, 106, 661-676.

Deit, L.L., Mangold, N., Forni, O., Cousin, A., Lasue, J., Schröder, S., Wiens, R.C., Sumner, D., Fabre, C., Stack, K.M., Anderson, R.B., Blaney, D., Clegg, S., Dromart, G., Fisk, M., Gasnault, O., Grotzinger, J.P., Gupta, S., Lanza, N., Mouélic, S.L., Maurice, S., Mclennan, S.M., Meslin, P.-Y., Nachon, M., Newsom, H., Payré, V., Rapin, W., Rice, M., Sautter, V., Treiman, A.H., 2016. The potassic sedimentary rocks in Gale Crater, Mars, as seen by ChemCam on board Curiosity. Journal of Geophysical Research: Planets 121, 784–804. doi:10.1002/2015je004987

Dorrell, R., 2010. Particulate Suspension: The Mechanics of Suspension and Deposition. PhD Thesis, University of Bristol, 228 pp.

Dorrell, R., Hogg, A. J., 2010. Sedimentation of bidisperse suspensions. International Journal of Multiphase Flow, 36(6), 481-490.

Dorrell, R. M., Hogg, A. J., 2011. Length and time scales of response of sediment suspensions to changing flow conditions. Journal of Hydraulic Engineering, 138(5), 430-439.

Dorrell, R. M., A. J. Hogg, D. Pritchard, 2013. Polydisperse suspensions: Erosion, deposition, and flow capacity. J. Geophys. Res. Earth Surf. 118, 1939-1955. doi.org/10.1002/jgrf.20129

Dorrell, R.M., Amy, L.A., Peakall, J., McCaffrey, W.D., 2018. Particle size distribution controls the threshold between net sediment erosion and deposition in suspended load dominated flows. Geophysical Research Letters 45, 1443-1452. doi:10.1002/2017gl076482

Dietrich, W. E., Palucis , M. C., Williams , R. M. ., Lewis , K. W., Rivera-Hernandez , F., Sumner, D.Y., 2017. Fluvial Gravels on Mars: Analysis and Implications. In: Gravel - Bed Rivers: Processes and Disasters, D. Tsutsumi & J. B. Laronne (eds.), 755-783, John Wiley & Sons Ltd. https://doi.org/10.1002/9781118971437.ch28

Edgar, L. A., Gupta, S., Rubin, D. M., Lewis, K. W., Kocurek, G. A., Anderson, R. B., Bell, J. F., Dromart, G., Edgett, K. S., Grotzinger, J. P., Hardgrove, C., Kah, L. C., Leveille, R., Malin, M. C., Mangold, N., Milliken, R. E., Minitti, M., Palucis, M., Rice, M., Rowland, S. K., Schieber, J., Stack, K. M., Sumner, D. Y., Wiens, R. C., Williams, R. M. E. and Williams, A. J., 2017. Shaler: in situ analysis of a fluvial sedimentary deposit on Mars. Sedimentology, 65, 96-122, doi.org/10.1111/sed.12370.

Ehlmann, B.L., et al., 2011. Subsurface water and clay mineral formation during the early history of Mars. Nature 479, 53. http://dx.doi.org/10.1038/nature10582.

Garcia, M. H., 2008. Sediment transport and morphodynamics. In M. H. Garcia (Ed.), Sedimentation engineering: Processes, measurements, modeling and practice. ASCE manuals and reports on engineering practice No. 110 (pp. 21–164). Reston, VA: American Society of Civil Engineers. https://doi.org/10.1061/9780784408148.ch02

Garcia, M. H., & Parker, G., 1991. Entrainment of bed sediment into suspension. Journal of Hydraulic Engineering, 117(4), 414–435. https://doi. org/10.1061/(ASCE)0733-9429(1991)117:4(414)

Garcia, M. H., & Parker, G., 1993. Experiments on the entrainment of sediment into suspension by a dense bottom current. Journal of Geophysical Research, 98(C3), 4793–4807. https://doi.org/10.1029/92JC02404

Giachetta, E., Willett, S.D., 2018. A global dataset of river network geometry. Scientific Data 5:180127. DOI: 10.1038/sdata.2018.127

Gilbert, G. K., Murphy, E. C., 1914. The transportation of debris by running water. U.S. Geological Survey Professional Paper 86, U.S. Government Printing Office, Washington, D.C. doi: 10.3133/pp86

Griffith, C.A., Penteado, P., Rannou, P., Brown, R., Boudon, V., Baines, K.H., Clark, R., Drossart, P., Buratti, B., Nicholson, P., McKay, C.P., Coustenis, A., Negrao, A., Jaumann, R., 2006. Evidence for a polar ethane cloud on Titan. Science 313, 1620–1622. doi:10.1126/science.1128245

Grotzinger, J., Arvidson, R., Bell, J., Calvin, W., Clark, B., Fike, D., . . . Watters, W., 2005. Stratigraphy and sedimentology of a dry to wet eolian depositional system, Burns formation, Meridiani Planum, Mars. Earth and Planetary Science Letters, 240(1), 11-72. doi:10.1016/j.epsl.2005.09.039

Grotzinger J. P., Hayes A. G., Lamb M. P., and McLennan S. M., 2013. Sedimentary processes on Earth, Mars, Titan, and Venus. In Comparative Climatology of Terrestrial Planets (S. J. Mackwell et al., eds.), pp. 439–472. Univ. of Arizona, Tucson, DOI: 10.2458/azu_uapress_9780816530595-ch18.

Hack, J. T., 1960. Interpretation of erosion topography in humid temperate regions: Am. Jour. Sci., 258A, 80–97.

Hayes, A.G., 2016. The lakes and seas of Titan. Annual Review of Earth and Planetary Sciences 44, 57–83. doi:10.1146/annurev-earth-060115-012247

Hayes, A.G., Lorenz, R.D., Lunine, J.I., 2018. A post-Cassini view of Titan's methane-based hydrologic cycle. Nature Geoscience 11, 306–313. doi:10.1038/s41561-018-0103-y

Hirano, M. (1971), River bed degradation with armoring [in Japanese], Proc. Jpn. Soc. Civil Eng., 195, 55–65.

Hiscott, R.N., 1994. Loss of capacity, not competence, as the fundamental process governing deposition from turbidity currents. J. Sediment. Res. A64, 209–214.

Hoke, M.R., Hynek, B.M., Achille, G.D., Hutton, E.W., 2014. The effects of sediment supply and concentrations on the formation timescale of Martian deltas. Icarus 228, 1–12. doi:10.1016/j.icarus.2013.09.017

Hsu, T.-J., Jenkins, J.T., Liu, P.L-F., 2004. On two-phase sediment transport: sheet flow of massive particles. Proceedings of the Royal Society A: Mathematical, Physical and Engineering Sciences 460, 2223–2250. doi:10.1098/rspa.2003.1273

Hynek, B. M., M. Beach, Hoke, M. R. T., 2010, Updated global map of Martian valley networks and implications for climate and hydrologic processes, J. Geophys. Res., 115, E09008, doi:10.1029/2009JE003548.

Imanaka, H., Khare, B.N., Elsila, J.E., Bakes, E.L., Mckay, C.P., Cruikshank, D.P., Sugita, S., Matsui, T., Zare, R.N., 2004. Laboratory experiments of Titan tholin formed in cold plasma at various pressures: implications for nitrogen-containing polycyclic aromatic compounds in Titan haze. Icarus 168, 344–366. doi:10.1016/j.icarus.2003.12.014

Irwin, R.P., Craddock, R.A., Howard, A.D., 2005. Interior channels in Martian valley networks: Discharge and runoff production. Geology 33, 489. doi:10.1130/g21333.1

Jacobsen, R. E., & Burr, D. M. (2017). Dichotomies in the fluvial and alluvial fan deposits of the Aeolis Dorsa, Mars: Implications for weathered sediment and paleoclimate. Geosphere, 13(6), 2154-2168. doi:10.1130/ges01330.1

Jones, A., Pickering, K., 2003. Evidence for aqueous fluid–sediment transport and erosional processes on Venus. Journal of the Geological Society 160, 319–327. doi:10.1144/0016-764902-111

Kleinhans, M.G., 2005. Flow discharge and sediment transport models for estimating a minimum timescale of hydrological activity and channel and delta formation on Mars. Journal of Geophysical Research 110. doi:10.1029/2005je002521

Kleinhans, M. G., H. Markies, S. J. de Vet, A. C. in 't Veld, and F. N. Postema (2011), Static and dynamic angles of repose in loose granular materials under reduced gravity, J. Geophys. Res., 116, E11004, doi:10.1029/2011JE003865

Kneller, B. & Buckee, C., 2000. he structure and fluid mechanics of turbidity currents: a review of some recent studies and their geological implications. Sedimentology, 47, 62-94.

Kneller, B., 2003. The influence of flow parameters on turbidite slope channel architecture. Marine and Petroleum Geology, 20(6-8), 901–910, doi.org/10.1016/j.marpetgeo.2003.03.001

Komar, P.D., 1979. Comparisons of the hydraulic of water flow in Martian outflow channels with flows of similar scale on Earth. Icarus 37, 156–181.

Komar, P.D., 1980. Modes of sediment transport in channelized water flows with ramifications to the erosion of the Martian outflow channels. Icarus 42, 317–329. doi:10.1016/0019-1035(80)90097-4

Konsoer, K., Zinger, J., Parker, G., 2013. Bankfull hydraulic geometry of submarine channels created by turbidity currents: Relations between bankfull channel characteristics and formative flow discharge. Journal of Geophysical Research: Earth Surface 118, 216–228. doi:10.1029/2012jf002422

Konsoer, K.M., Leroy, J., Burr, D., Parker, G., Jacobsen, R., Turmel, D., 2018. Channel slope adjustment in reduced gravity environments and implications for Martian channels. Geology 46, 183–186. doi:10.1130/g39666.1

Kostaschuk, R., Shugar, D., Best, J., Parsons, D., Lane, S., Hardy, R., Orfeo, O., 2009. Suspended sediment transport and deposition over a dune: Río Paraná, Argentina. Earth Surf. Process. Landforms 34, 1605–1611.

Krumbein, W. C., 1934. Size frequency distributions of sediments. Journal of Sedimentary Petrology, 2, 65-77. doi:10.1306/D4268EB9-2B26-11D7-8648000102C1865D.

Kumbhakar, M.,Kundu, S., Ghoshal, K., 2018. An explicit analytical expression for bed-load layer thickness based on maximum entropy principle. Physics Letters A, 382, 2297-2304.

Lamb, M. P., Grotzinger, J. P., Southard, J. B., & Tosca, N. J., 2012. Were Aqueous Ripples on Mars Formed by Flowing Brines? Sedimentary Geology of Mars, 139-150. doi:10.2110/pec.12.102.0139

Lapôtre, M. G. A., Lelpi, A., Lamb, M. P., Williams, R. M. E., & Knoll, A. H., 2019. Model for the formation of single - thread rivers in barren landscapes and implications for pre - Silurian and Martian fluvial deposits. Journal of Geophysical Research: Earth Surface, 124, 2757-2777, https://doi.org/10.1029/2019JF005156

Lacey, G., 1930. Stable channels in alluvium: Proc. ICE, 229, 259–270.

Leeder, M.R., 1982. Sedimentology: Process and Product. Chapman and Hall, 344 pp.

Leeder, M.R., Gray, T.E., Alexander, J., 2005. Sediment suspension dynamics and a new criterion for the maintenance of turbulent suspensions. Sedimentology 52, 683–691. doi:10.1111/j.1365-3091.2005.00720.x

Leopold, L. B., & Wolman, M. G., 1957. River channel patterns: braided, meandering, and straight. U.S. Geological Survey Professional Paper 282-B. U.S. Government Printing Office, Washington, D.C. doi:10.3133/pp282B

Lorenz, R.D., Lunine, J.I., 2005. Titan's surface before Cassini. Planet. Space. Sci. 53, 557-576.

Lorenz, R. D. et al., 2006. The Sand Seas of Titan: Cassini RADAR Observations of Longitudinal Dunes. Science, 312(5774), 724-727. doi:10.1126/science.1123257

Lorenz, R.D., Lopes, R.M., Paganelli, F., Lunine, J.I., Kirk, R.L., Mitchell, K.L., Soderblom, L.A., Stofan, E.R., Ori, G., Myers, M., Miyamoto, H., Radebaugh, J., Stiles, B., Wall, S.D., Wood, C., 2008. Fluvial channels on Titan: Initial Cassini RADAR observations. Planetary and Space Science 56, 1132–1144. doi:10.1016/j.pss.2008.02.009

Lunine, J.I., Stevenson, D.J., Yung, Y.L., 1983. Ethane ocean on Titan. Science 222, 1229–1230. doi:10.1126/science.222.4629.1229

Mackin, J. H., 1948, Concept of the graded river: Geol. Soc. America Bull., v. 59, p. 463–512.

van Maren, D.S.V., Winterwerp, J.C., Wang, Z.Y., Pu, Q., 2009. Suspended sediment dynamics and morphodynamics in the Yellow River, China. Sedimentology 56, 785–806. doi:10.1111/j.1365-3091.2008.00997.x

Matsubara Y., Howard A. D, Burr, D.M., Rebecca M.E., Williams, M.E., Dietrich W.E., Moore J.M., 2015. River meandering on Earth and Mars: A comparative study of Aeolis Dorsa meanders, Mars and possible terrestrial analogs of the Usuktuk River, AK, and the Quinn River, NV. Geomorphology 240, 102–120, doi.org/10.1016/j.geomorph.2014.08.031.

Mclean, S.R., 1992. On the calculation of suspended load for noncohesive sediments. Journal of Geophysical Research 97, 5759. doi:10.1029/91jc02933

McSween, H. Y. Jr., Moersch, J. E., Burr, D. M., Emery, J. P., Kah, L. C., McCanta, M. C., 2019. Planetary Geoscience. Cambridge University Press, 350 pp. ISBN: 9781107145382

Middleton, G.V., 1970. Generation of the Log-Normal Frequency Distribution in Sediments. In: Romanova M.A., Sarmanov O.V. (eds) Topics in Mathematical Geology, 34-. Springer, Boston, MA.

Middleton, G.V., Southard, J.B., 1984. Mechanics of Sediment Movement. SEPM. Short Course, 3, 401pp.

Miller, M.C. & Komar, P.D., 1977. The development of sediment threshold curves for unusual environments (Mars) and for inadequately studied materials (terran sands). Sedimentology, 24, 709-721.

Milliman, J. D., Meade, R. H., 1983. World-wide delivery of river sediment to the oceans. The Journal of Geology, 91, 1-21.

Misiura, K., Czechowski., L., 2015. Numerical modelling of sedimentary structures in rivers on Earth and Titan. Geological Quarterly, 59. 563-580, doi: http://dx.doi.org/10.7306/gq.1236

Moore, J. M., 2005. Large alluvial fans on Mars. Journal of Geophysical Research, 110(E4). doi:10.1029/2004je001352

Morgan, A. M., & Craddock, R. A., 2019. Assessing the accuracy of paleodischarge estimates for rivers on Mars. Geophysical Research Letters, 46, 11, 738-11,746, https://doi.org/10.1029/2019GL084921

Naqshband, S., Hoitink, A. J. F., McElroy, B., Hurther, D., & Hulscher, S. J. M. H., 2017. A sharp view on river dune transition to upper stage plane bed. Geophysical Research Letters, 44, 11,437–11,444. https://doi.org/10.1002/2017GL075906

Niño, Y., Lopez, F., & Garcia, M., 2003. Threshold for particle entrainment into suspension. Sedimentology, 50(2), 247-263. doi:10.1046/j.1365-3091.2003.00551.x

Ori, G.G., Marinangeli, L., Baliva, A., Bressan, M., Strom, R.G., 1998. Fluid dynamics of liquids on Titans surface. Planetary and Space Science 46, 1417–1421. doi:10.1016/s0032-0633(97)00125-6

Parker, G., C. Paola, and S. Leclair, 2000, Probabilistic Exner sediment continuity equation for mixtures with no active layer, J. Hydraul. Eng.,126, 818–826.

Parker, G., Wilcock, P. R., Paola, C., Dietrich, W. E., & Pitlick, J., 2007. Physical basis for quasi-universal relations describing bankfull hydraulic geometry of single-thread gravel bed rivers. Journal of Geophysical Research, 112(F4). doi:10.1029/2006jf000549

Parsons, A. J., Cooper, J., & Wainwright, J., 2015. What is suspended sediment? Earth Surface Processes and Landforms, 40(10), 1417-1420. doi:10.1002/esp.3730

Perron, J. T., M. P. Lamb, C. D. Koven, I. Y. Fung, E. Yager, M. Ádámkovics, 2006. Valley formation and methane precipitation rates on Titan, J. Geophys. Res., 111, E11001, doi:10.1029/2005JE002602.

van Rijn, L. C., 1984a. Sediment transport, part I: bed load transport, J. Hydraul. Eng., 110(10), 1431–1456.

van Rijn, L. C., 1984b. Sediment transport, part II: suspended load transport, J. Hydraul. Eng., 110(11), 1613–1641.

Rodriguez, J. A., Kargel, J. S., Baker, V. R., Gulick, V. C., Berman, D. C., Fairén, A. G., . . . Glines, N. (2015). Martian outflow channels: How did their source aquifers form and why did they drain so rapidly? Scientific Reports, 5(1). doi:10.1038/srep13404

Rouse, H., 1937. Modern conceptions of the mechanics or fluid turbulence. Transactions of the American Society of Civil Engineers, 102, 463–505.

Shields, A., 1936. Anwendung der Aehnlichkeitsmechanik und der Turbulenzforschung auf die Geschiebebewegung. Berlin: Preussischen Versuchsanstalt für Wasserbau.

Schon, S.C., Head, J.W., Fassett, C.I., 2012. An overfilled lacustrine system and progradational delta in Jezero crater, Mars: Implications for Noachian climate. Planetary and Space Science 67, 28–45. doi:10.1016/j.pss.2012.02.003

Schieber, J., Bish, D., Coleman, M., Reed, M., Hausrath, E. M., Cosgrove, J., . . . Malin, M. (2016). Encounters with an unearthly mudstone: Understanding the first mudstone found on Mars. Sedimentology, 64(2), 311-358. doi:10.1111/sed.12318

Schröder, S. and Keller, H., 2008, The reflectance spectrum of Titan's surface at the Huygens landing site determined by the descent imager/spectral radiometer: Planetary and Space Science, 56, 753–769, doi:10.1016/j.pss.2007.10.011.

Schumm, S.A., 1985. Patterns of alluvial rivers. Annual Review of Earth and Planetary Sciences, 13, 5-27.

Smith, J. D., & Hopkins, T. S., 1973. Sediment transport on the continental shelf off of Washington and Oregon in light of recent current measurements. In D. J. P. Swift, D. B. Duane, & O. H. Pilkey (Eds.), Shelf sediment transport: Process and patterns (pp. 143–179). Stroudsburg, PA: Hutchinson and Ross.

Soulsby, R., 1997. Dynamics of marine sands: A manual for practical applications. UK: Thomas Telford Publications.

Sumer, B.M., Kozakiewicz, A.., Fredsøe, J., Deigaard, R., 1996. Velocity and concentration profiles in sheet-flow layer of movable bed. Journal of Hydraulic Engineering, 122, 549-558.

Syvitski, J. P., S. D. Peckham, R. Hilberman and T. Mulder, 2003. Predicting the terrestrial flux of sediment to the global ocean: a planetary perspective. Sediment. Geol. 162, 5-24. doi.org/10.1016/S0037-0738(03)00232-X

Tomasko, M., Archinal, B., Becker, T. et al. Rain, winds and haze during the Huygens probe's descent to Titan's surface. Nature 438, 765–778 (2005). https://doi.org/10.1038/nature04126

Turowski, J. M., Rickenmann, D., & Dadson, S. J., 2010. The partitioning of the total sediment load of a river into suspended load and bedload: A review of empirical data. Sedimentology, 57(4), 1126-1146. doi:10.1111/j.1365-3091.2009.01140.x

Waite, J.H., Jr., Young, D.T., Westlake, J.H., Lunine, J.I., McKay, C.P., and Lewis, W.S., 2009, High-altitude production of Titan's aerosols, in Brown, R.H., Lebreton , J.-P., and Waite, J.H., Jr., eds., Titan from Cassini-Huygens: Dordrecht, Heidelberg, Springer, p. 201–214.

Williams, R. M., Grotzinger, J. P., Dietrich, W. E., Gupta, S., Sumner, D. Y., Wiens, R. C., . . . Moores, J. E., 2013. Martian Fluvial Conglomerates at Gale Crater. Science, 340(6136), 1068-1072. doi:10.1126/science.1237317

Wood, L.J., 2006. Quantitative geomorphology of the Mars Eberswalde delta. Geological Society of America Bulletin 118, 557–566. doi:10.1130/b25822.1

Velikanov, M. A., 1954. Gravitational theory of sediment transport. Journal of Science of the Soviet Union, Geophysics, 4.

Villanueva, G.L., Mumma, M.J., Novak, R.E., Kaufl, H.U., Hartogh, P., Encrenaz, T., Tokunaga, A., Khayat, A., Smith, M.D., 2015. Strong water isotopic anomalies in the Martian atmosphere: Probing current and ancient reservoirs. Science 348, 218–221. doi:10.1126/science.aaa3630

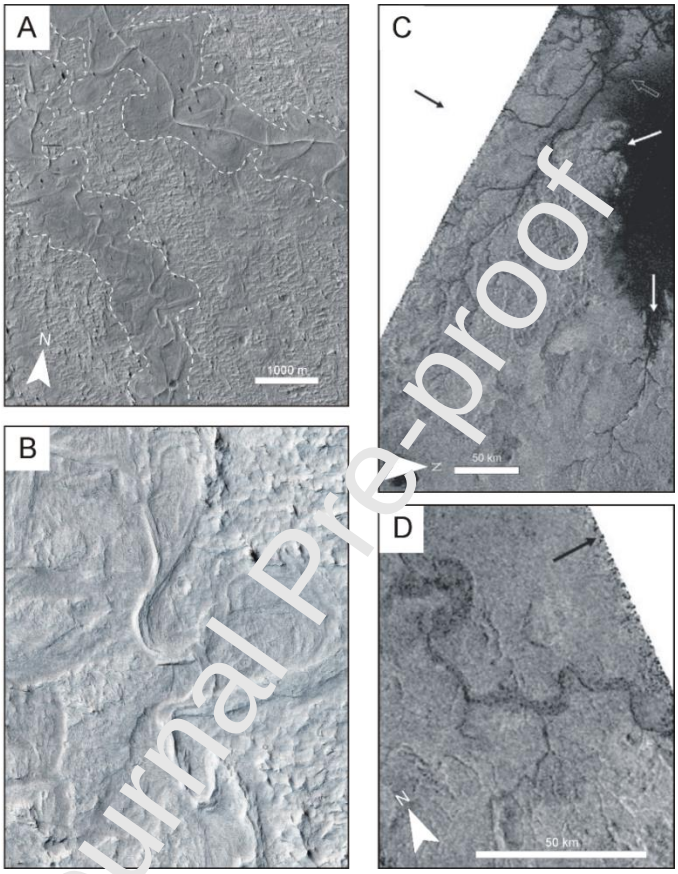

Figure 1. Channels on Mars and Titan. A) Wind-eroded sinuous ridges (between white dashed lines) inferred to be ancient meander belts, southern Aeolis Dorsa, Mars. B) Detail of left ridge in A showing patterns similar to terrestrial fluvial scroll bars, including chute channels associated with meander cutoff. C) Narrow, long, radar-dark features on Titan inferred to be fluvial channels located close to Lake Ligeia Mare (large oval dark area) with possible drowned valleys (white arrows). D) Sinuous long, radar-dark feature on Titan hypothesized to be an incised bedrock channel or confined meandering river. Images in A and B are from the High Resolution Imaging Science Experiment (HiRISE) camera (image PSP_010322_1740) courtesy of NASA/JPL/University of Arizona. Images in C and D are synthetic aperture radar (SAR) data from the *Cassini* Titan Radar Mapper (RADAR) from Burr et al. (2013). *[Permission to republish images in C and D will be sought]*

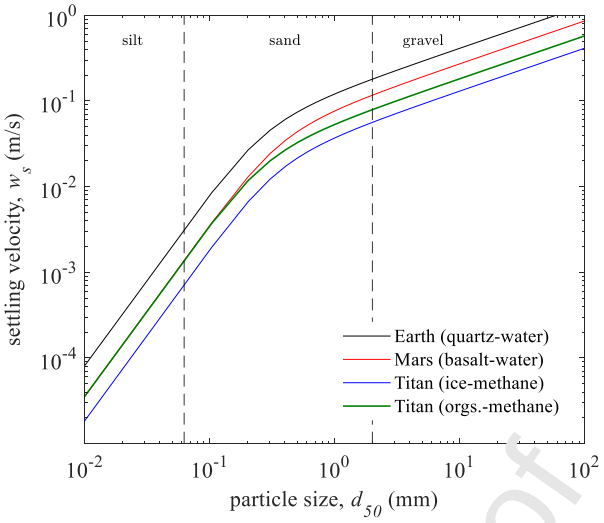

Figure 2. Settling velocity of quartz on Earth, basalt on Mars and ice and organic particles on Titan, calculated using Eq. (3).

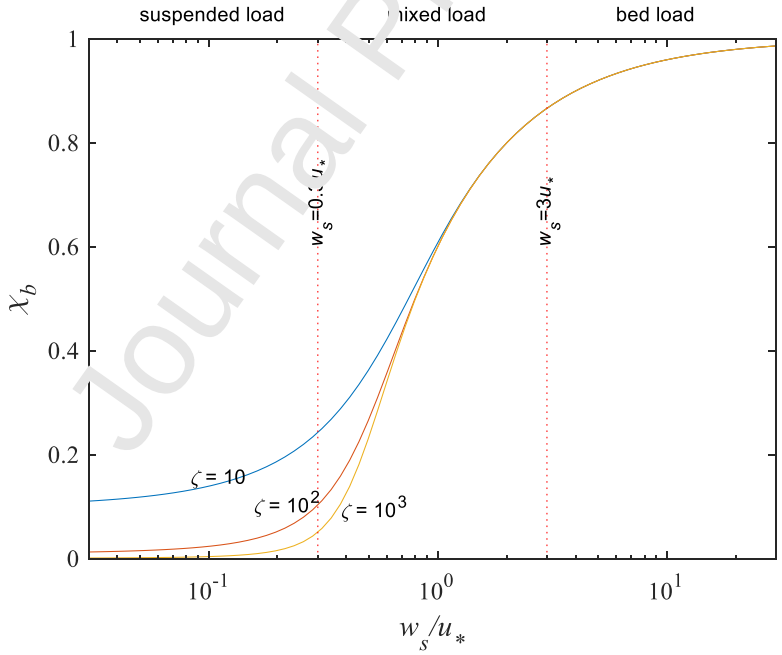

Figure 3. The fraction of total sediment load carried as bedload as a function of the ratio of the settling velocity to the shear velocity, w_s/u_*, and the relative depth, $\xi = h/z^+$ (after Dade and Friend, 1998). Sediment transport modes indicated are those used by Dade and Friend (1998).

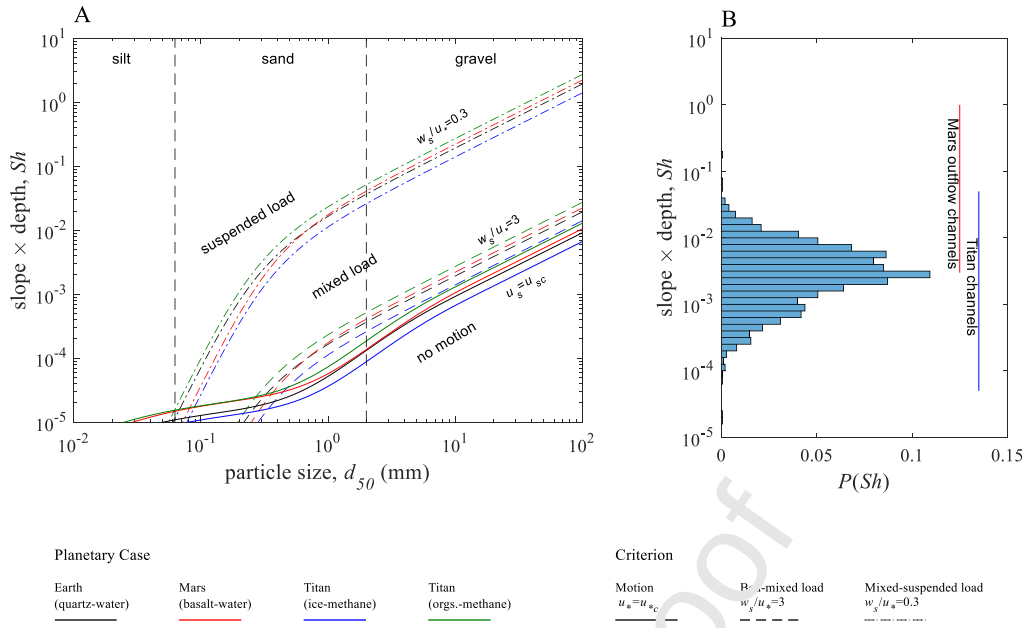

Figure 4. A) Sediment transport modes as a function of particle size, slope-depth product. B) Distribution of slope-depth product based on Earth river data (Dunne & Jerolmack, 2018). Vertical lines indicate ranges in slope-depth product estimated for Martian outwash channels (Komar, 1980; Wilson et al., 2004) and for channels on Titan (Perron et al., 2006).

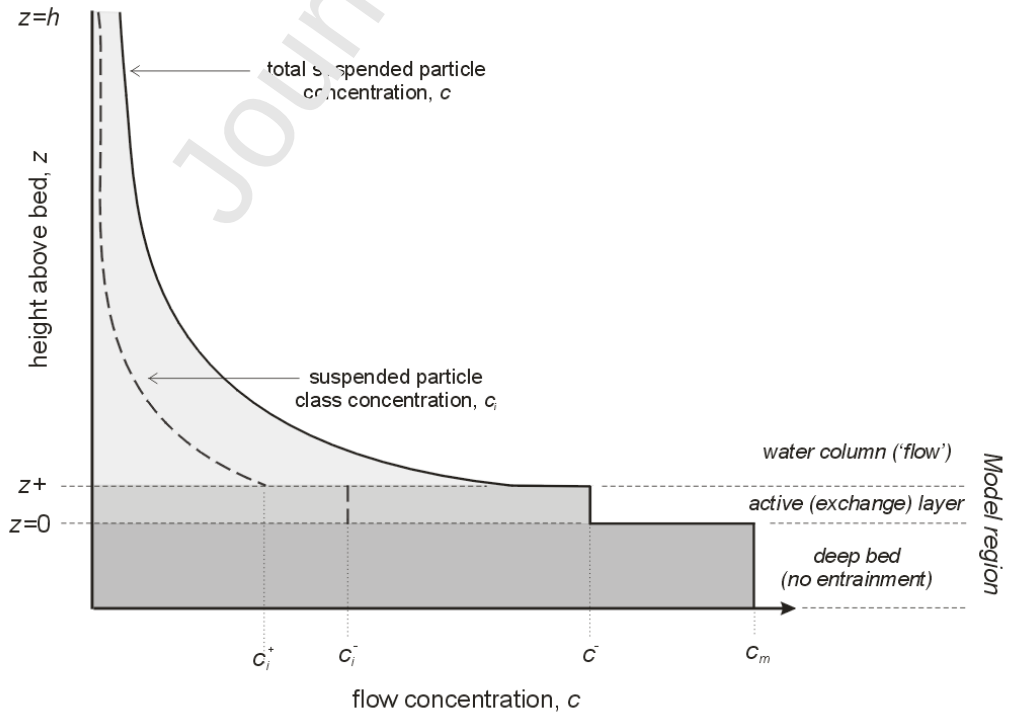

Figure 5. Schematic description of the flow power flux balance model, showing the principal model regions and example variations in the concentration of a single particle class and the total concentration with height above the bed (not to scale). Note that the particle class concentration in lower layer(s) does not necessarily exceed that of the overlying layer.

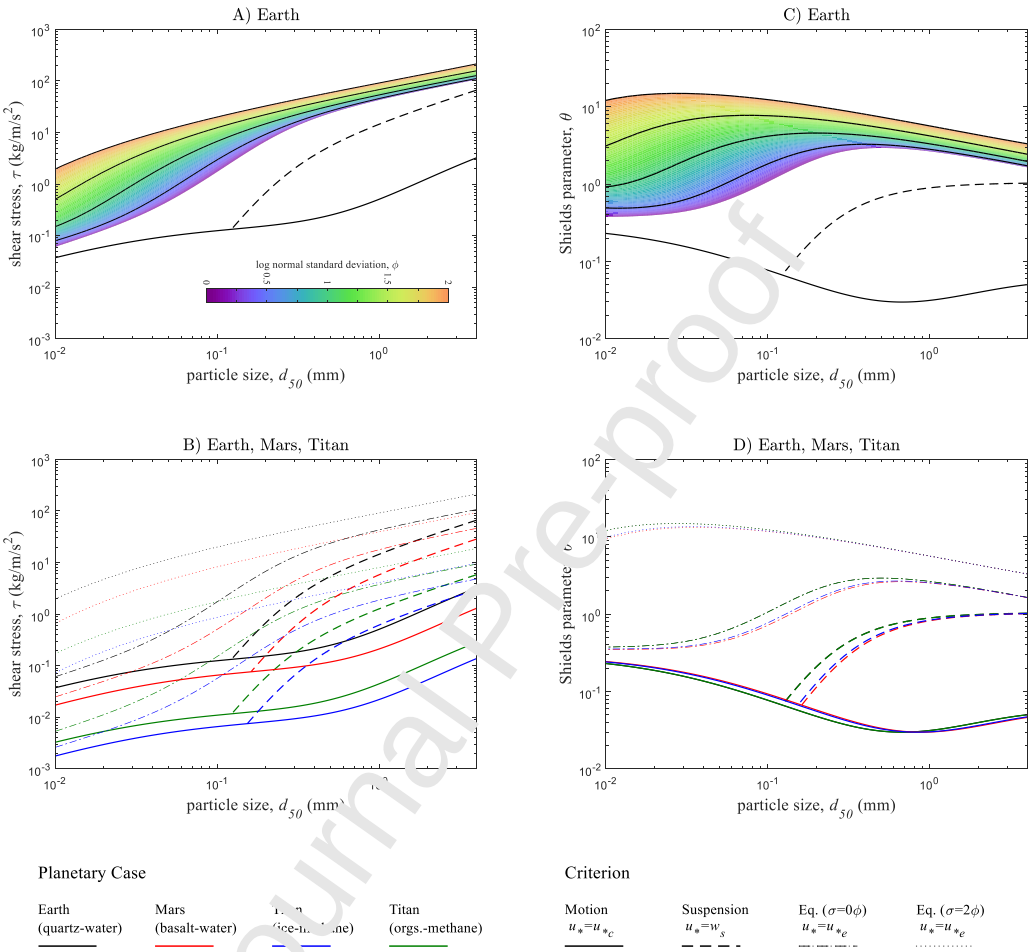

Figure 6. Shear stress (A-B) and Shields parameter (C-D) required for the threshold of initial motion, suspension and equilibrium conditions given variable particle size. Equilibrium model concentration, $c = 0.1\%$ and flow depth, $h = 1$. Particle standard deviation, σ, is in phi units, $\phi = -log_2(d)$ where d is particle size in mm.

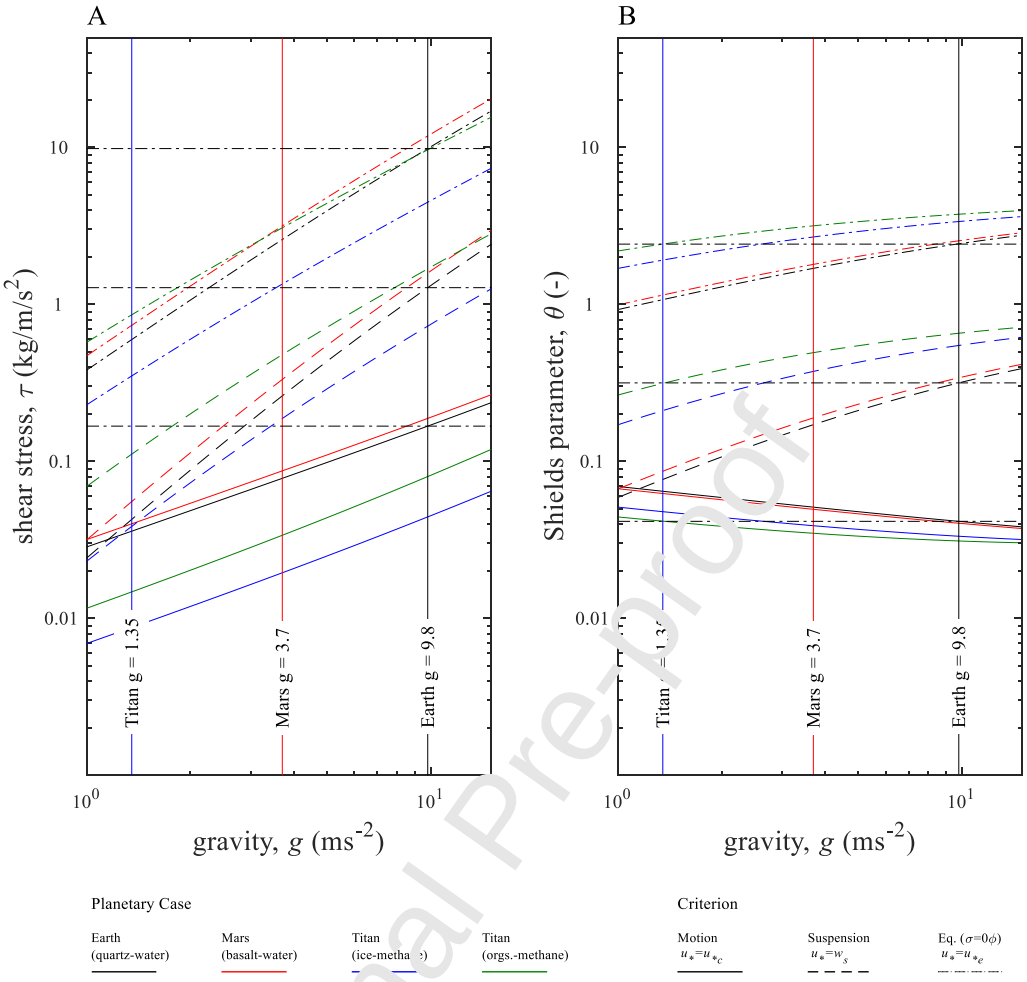

Figure 7. Shear stress (A) and Shields parameter (B) required for particle motion, suspension and equilibrium versus gravity. Horizontal dash-dot lines indicates values for Earth. Model median particle size, $d_{50} = 250\ \mu m$, concentration, $c = 0.1\%$, flow depth, $h = 1$, and particle standard deviation, $\sigma = 0$.

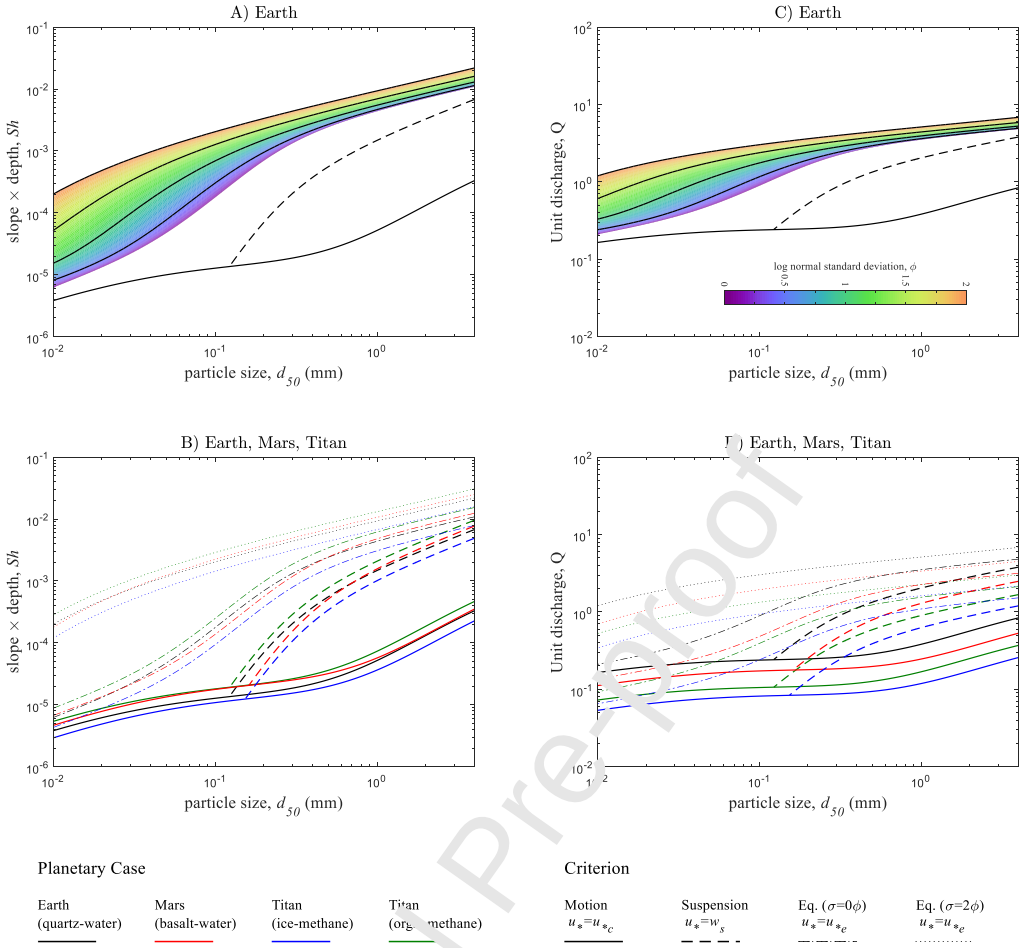

Figure 8. Slope-depth product or slope for $h = 1$ (A-B) and discharge (C-D) required for equilibrium conditions given variable particle size and standard deviation. Equilibrium model concentration, $c = 0.1\%$ and flow depth, $h = 1$. Particle standard deviation, σ, is in phi units, $\phi = -log_2(d)$ where d is particle size in mm.

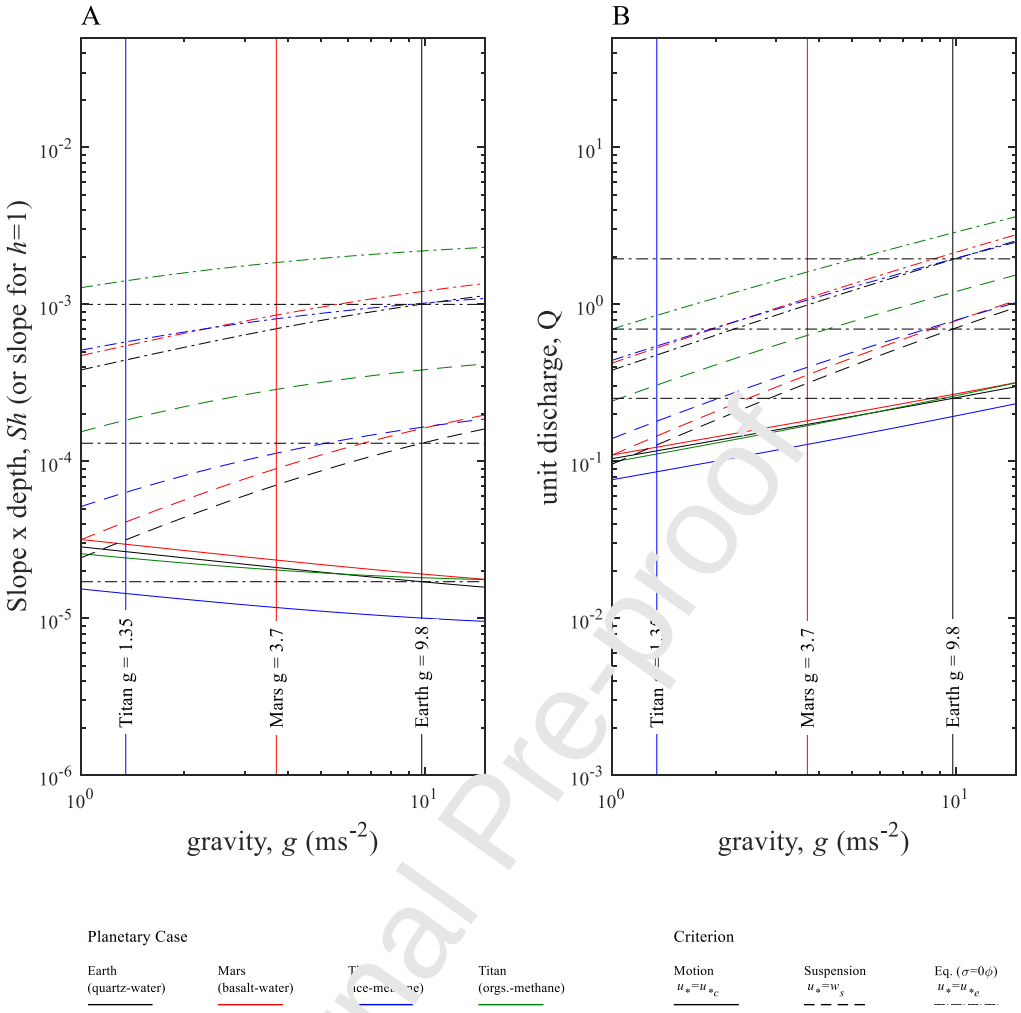

Figure 9. Slope-depth product (A) and unit discharge (B) required for particle motion, suspension and equilibrium versus gravity. Horizontal dash-dot lines indicates values for Earth. Model median particle size, $d_{50} = 250\,\mu m$, concentration, $c = 0.1\%$, flow depth, $h = 1$, and particle standard deviation, $\sigma = 0$.

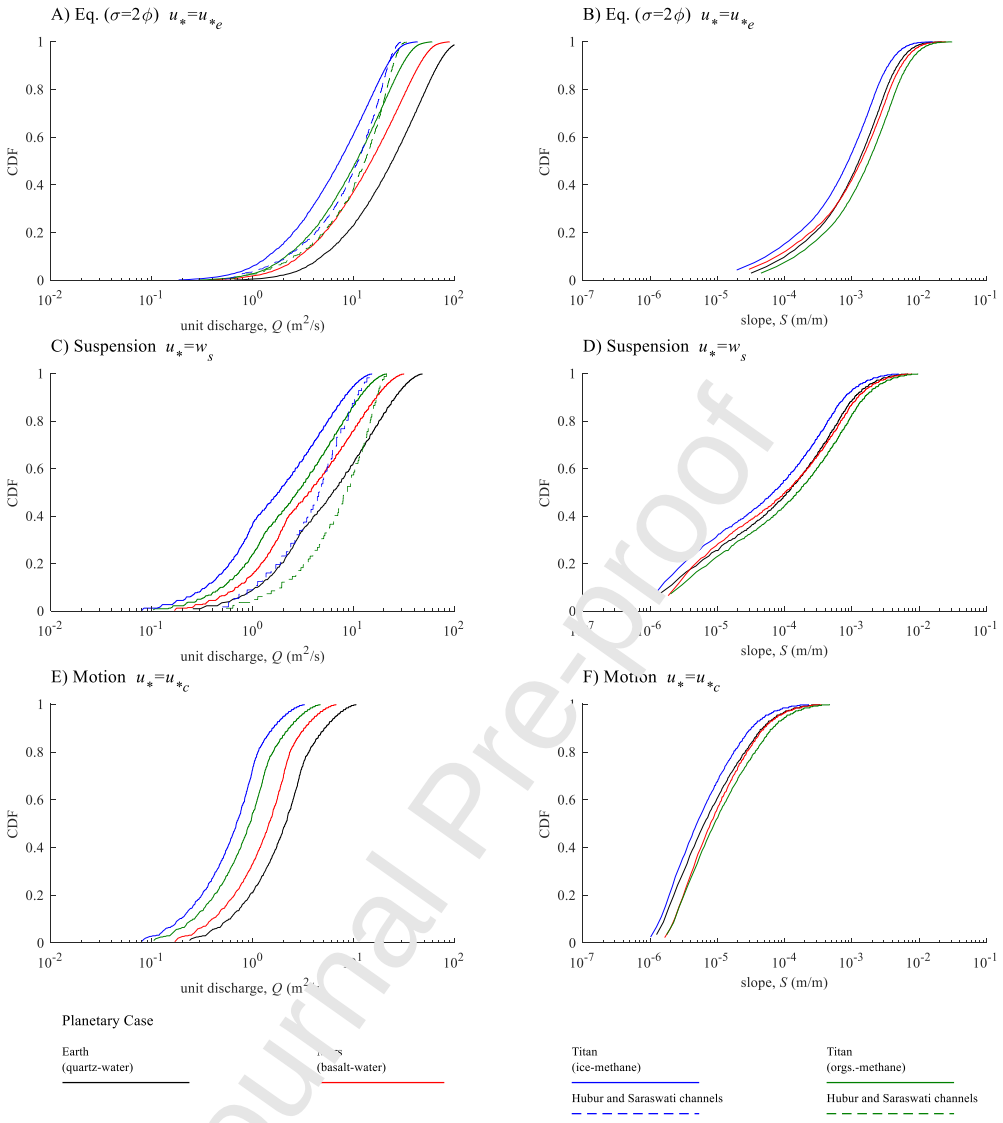

Figure 10. Cumulative probability of unit discharge and slope based on 2000 evaluations of equilibrium flow (A, B), threshold of suspension (C, D) and threshold of motion (E, F) given equally sampled values of flow depth, $1 < h < 10$, median particle size, $-2\phi < d_{50} < 4\,\phi$, and particle size distribution, $0.01 < \sigma < 2$, for $c = 0.1\%$. Results constrained for slopes in the range 1 x 10^{-3} ± 50%, appropriate for the Titanian Hubur and Saraswati channels are shown as dashed lines.

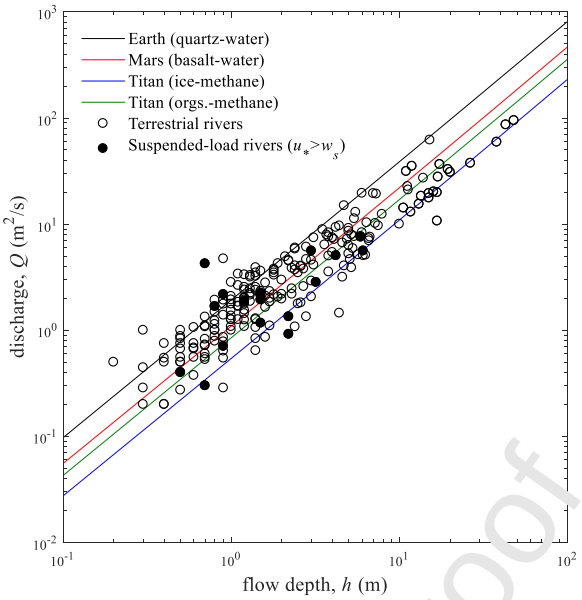

Figure 11. Equilibrium unit discharge versus flow depth for Earth, Mars and Titan cases (Table 1). Model concentration, $c = 0.1\%$, median particle size, $d_{50} = 250\,\mu m$ and for a flow depth, $h = 1\,m$. Circles show empirical data reported by Konsoer et al. (2018) for terrestrial rivers based on measured bankfull values; filled circles for rivers predicted to carry large proportions of suspended-load material based on $u_* > w_s$.

Supplementary figures

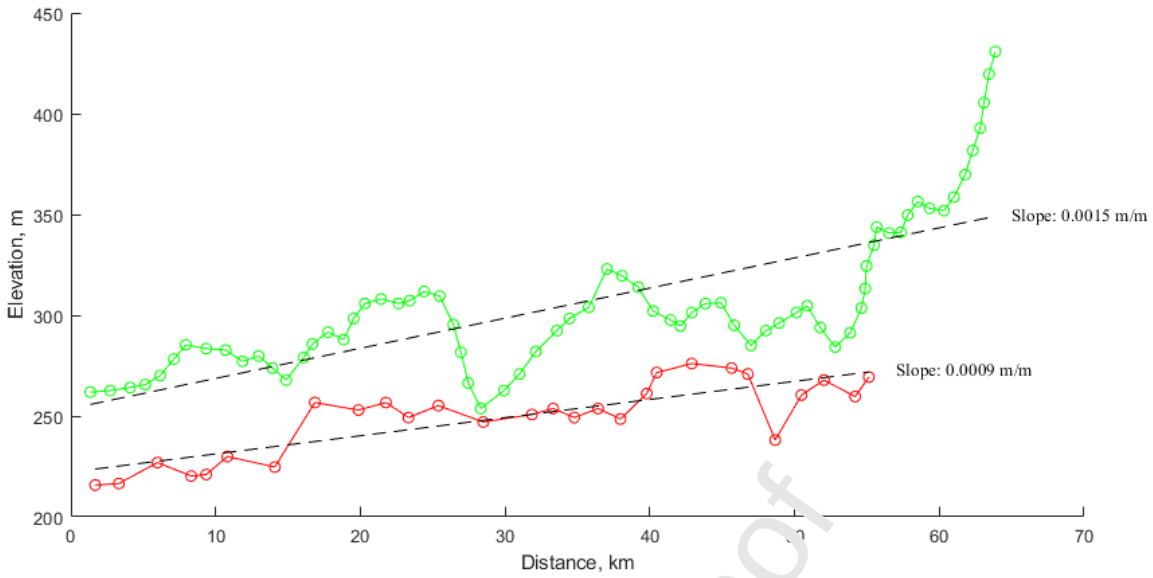

Figure S1. Mapped elevation profiles of the Hubur (green) and Saraswati (red) streams on Titan (based on data from Dhingra et al., 2018). Dashed lines show average slope based on linear best-fit of the elevation data.

	Earth	Mars	Titan	Titan
Gravity				
g, ms^{-2}	9.80	3.71	1.35	1.35
Fluid	Water	Water	CH_4/N_2	CH_4/N_2
ρ, kgm^{-3}	1000	1000	450	450
μ, Pa s	1×10^{-3}	1×10^{-3}	2×10^{-4}	2×10^{-4}
Sediment	Quartz	Basalt	Water ice	Organics
ρ_s, kgm^{-3}	2650	2900	992	1500
$r = \Delta\rho/\rho$	1.65	1.90	1.20	2.33

Table 1. Physical values used for modelling sediment transport on Earth, Mars and Titan taken from Burr et al. (2006) in which supporting references can be found.

Criterion	Dimensional shear stress	Dimensionless shear stress,	Shear velocity	Reference
Initial motion	$\tau_c = \theta_c\, g\Delta\rho d$	$\theta_c = \frac{0.3}{1+1.2D_s} + 0.055(1 - e^{-0.02D_s})$	$u_{*c} = \sqrt{\frac{g\Delta\rho d\theta_c}{\rho}}$	Shields (1936)
Suspension (suspended load-bedload transition)	$\tau_s = \rho {u_{*s}}^2$	$\theta_s = \frac{\rho {u_{*s}}^2}{g\Delta\rho d}$	$u_{*s} = w_s$	Bagnold (1966)
Suspended-load-dominated flow	$\tau_{\tilde{s}} = \rho {u_{*\tilde{s}}}^2$	$\theta_{\tilde{s}} = \frac{\rho {u_{*\tilde{s}}}^2}{g\Delta\rho d}$	$u_{*\tilde{s}} = w_s/0.3$	Dade & Friend (1998)
Suspended-load equilibrium sediment transport (erosion-deposition threshold)	$\tau_e = \rho\left(\frac{g\Delta\rho c w_s h}{\rho\lambda\varepsilon}\right)^{\frac{2}{3}} + \theta_c g\Delta\rho d$	$\theta_e = \frac{\tau_e}{g\Delta\rho d}$	$u_{*e} = \sqrt{\tau_e/\rho}$	Dorrell et al. (2018)

Table 2. Model formulae for sediment transport criteria.

Highlights

- New theory applied to understand sediment transport on different planetary bodies
- Indicate large variations in required shear stresses for sediment transport
- Effects of gravity compensate resulting in only moderate variation in equilibrium slope and flow depth
- Lower equilibrium slopes and discharges predicted for basalt-water systems on Mars and water ice-methane systems on Titan

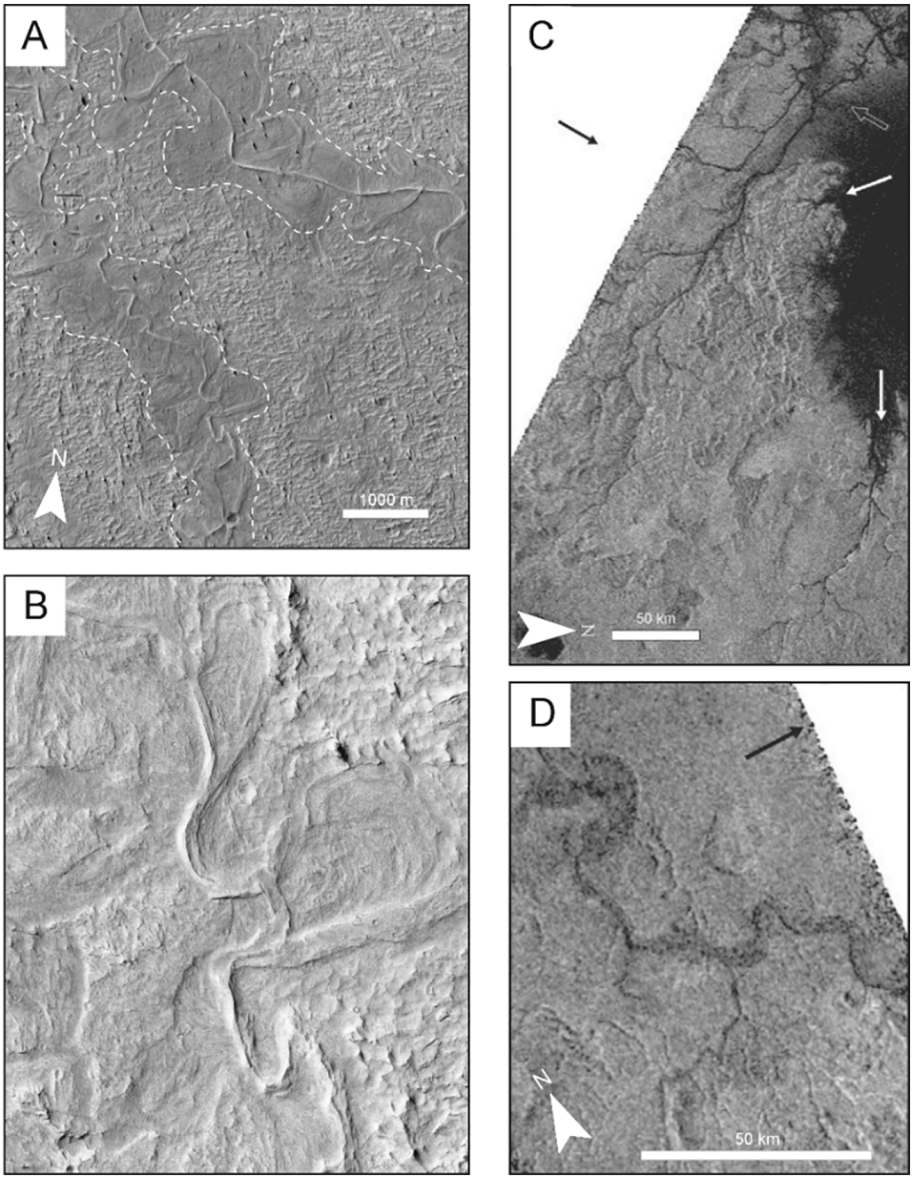

Figure 1

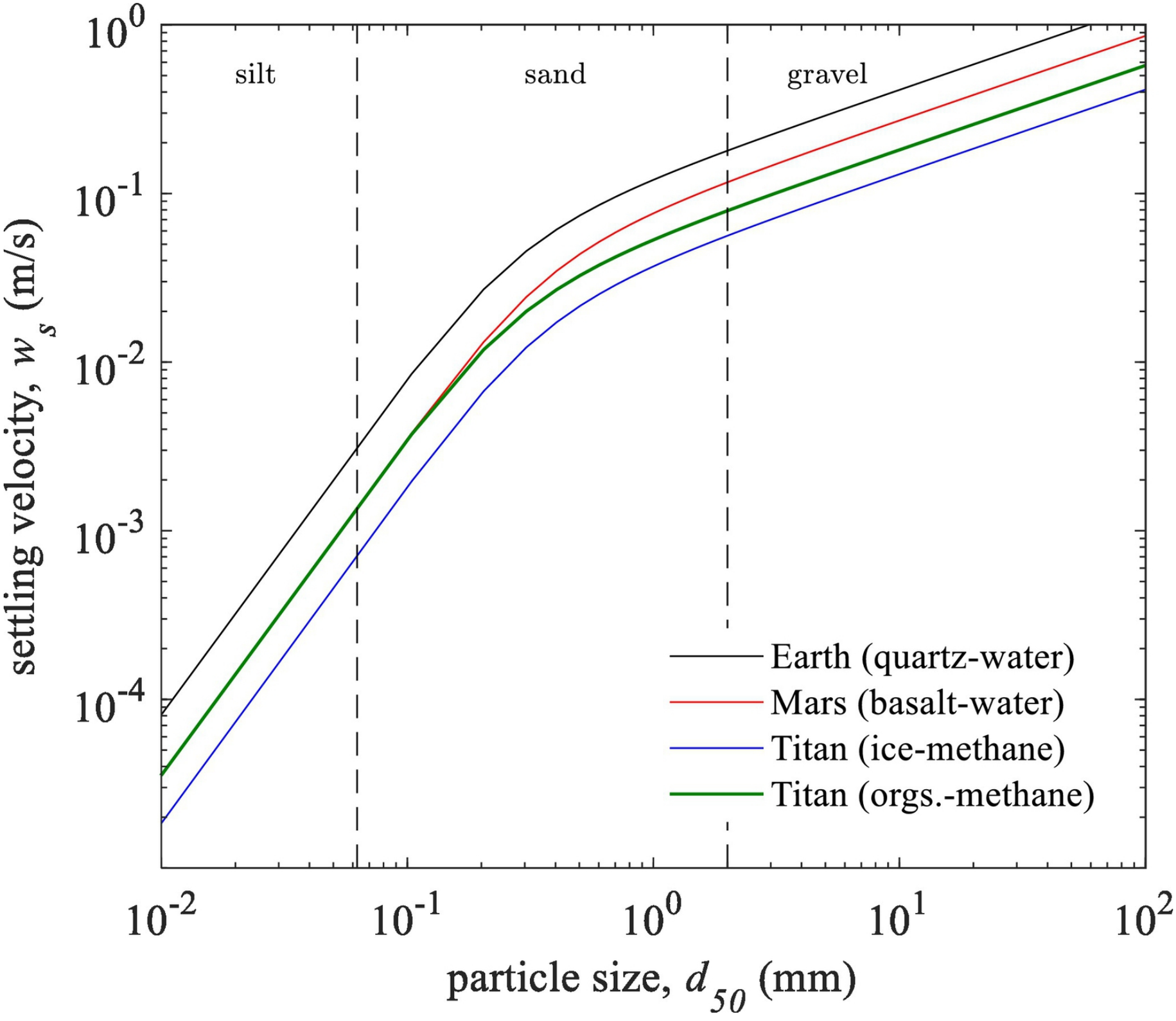
silt
sand
gravel
Earth (quartz-water)
Mars (basalt-water)
Titan (ice-methane)
Titan (orgs.-methane)
settling velocity, w_s (m/s)
particle size, d_{50} (mm)
10^0
10^{-1}
10^{-2}
10^{-3}
10^{-4}
10^{-2}
10^{-1}
10^0
10^1
10^2

Figure 2

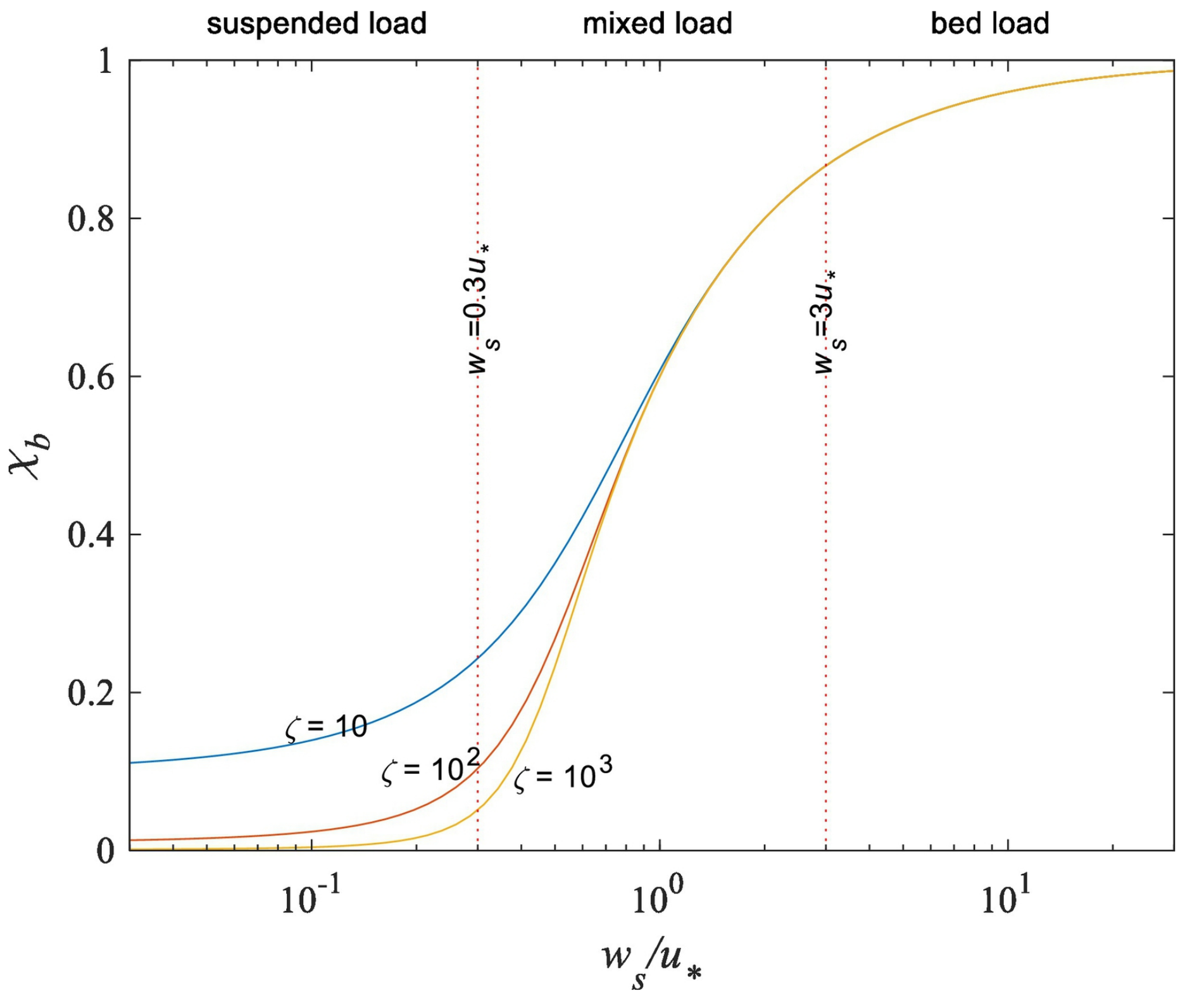
suspended load
mixed load
bed load
1
0.8
0.6
0.4
0.2
0
χ_b
w_s=0.3u_*
w_s=3u_*
ζ = 10
ζ = 10^2
ζ = 10^3
10^{-1}
10^0
10^1
w_s/u_*

Figure 3

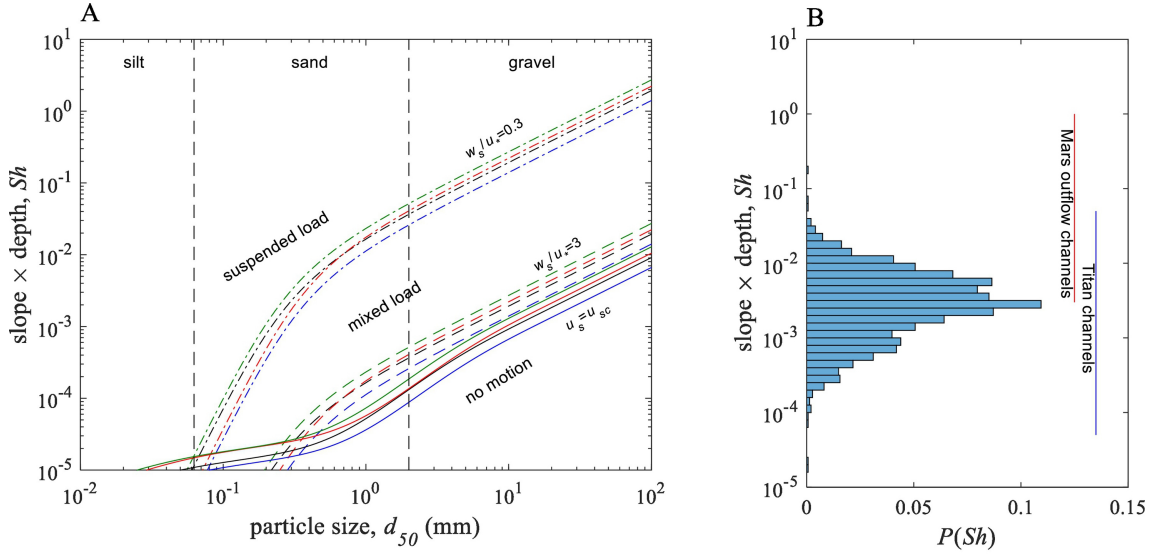
A
silt
sand
gravel
suspended load
mixed load
no motion
$w_s/u_*=0.3$
$w_s/u_*=3$
$u_s=u_{sc}$
slope × depth, Sh
particle size, d_{50} (mm)
B
Mars outflow channels
Titan channels
P(Sh)
Planetary Case
Earth (quartz-water)
Mars (basalt-water)
Titan (ice-methane)
Titan (orgs.-methane)
Criterion
Motion $u_*=u_{*_c}$
Bed-mixed load $w_s/u_*=3$
Mixed-suspended load $w_s/u_*=0.3$

Figure 4

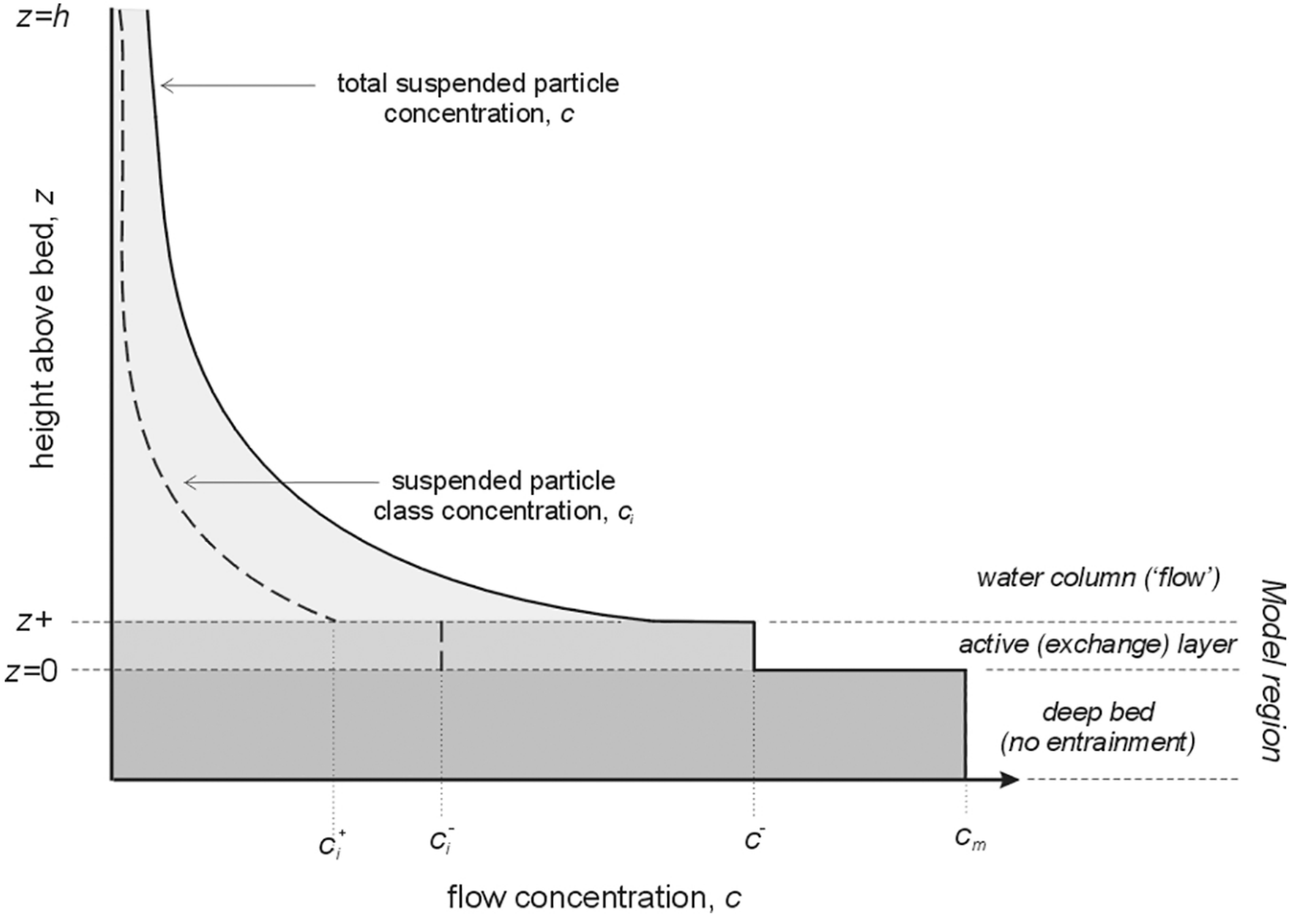
z=h
total suspended particle concentration, c
height above bed, z
suspended particle class concentration, c_i
water column ('flow')
z+
active (exchange) layer
z=0
deep bed (no entrainment)
Model region
c_i^+
c_i^-
c^-
c_m
flow concentration, c

Figure 5

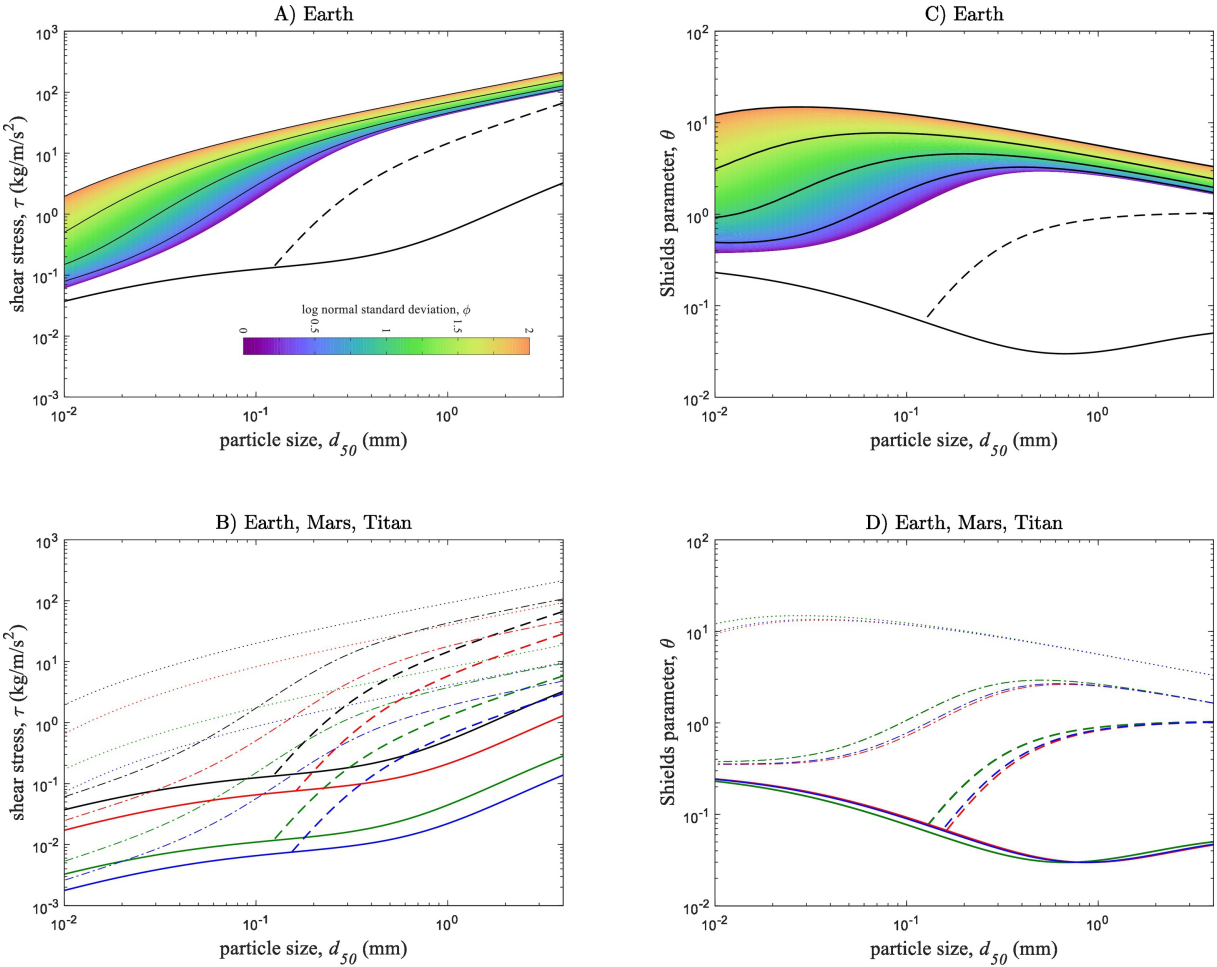
A) Earth
shear stress, τ (kg/m/s^2)
particle size, d_{50} (mm)
log normal standard deviation, ϕ
0
0.5
1
1.5
2
C) Earth
Shields parameter, θ
particle size, d_{50} (mm)
B) Earth, Mars, Titan
shear stress, τ (kg/m/s^2)
particle size, d_{50} (mm)
D) Earth, Mars, Titan
Shields parameter, θ
particle size, d_{50} (mm)
Planetary Case
Earth (quartz-water)
Mars (basalt-water)
Titan (ice-methane)
Titan (orgs.-methane)
Criterion
Motion $u_*=u_{*c}$
Suspension $u_*=w_s$
Eq. (σ=0ϕ) $u_*=u_{*e}$
Eq. (σ=2ϕ) $u_*=u_{*e}$

Figure 6

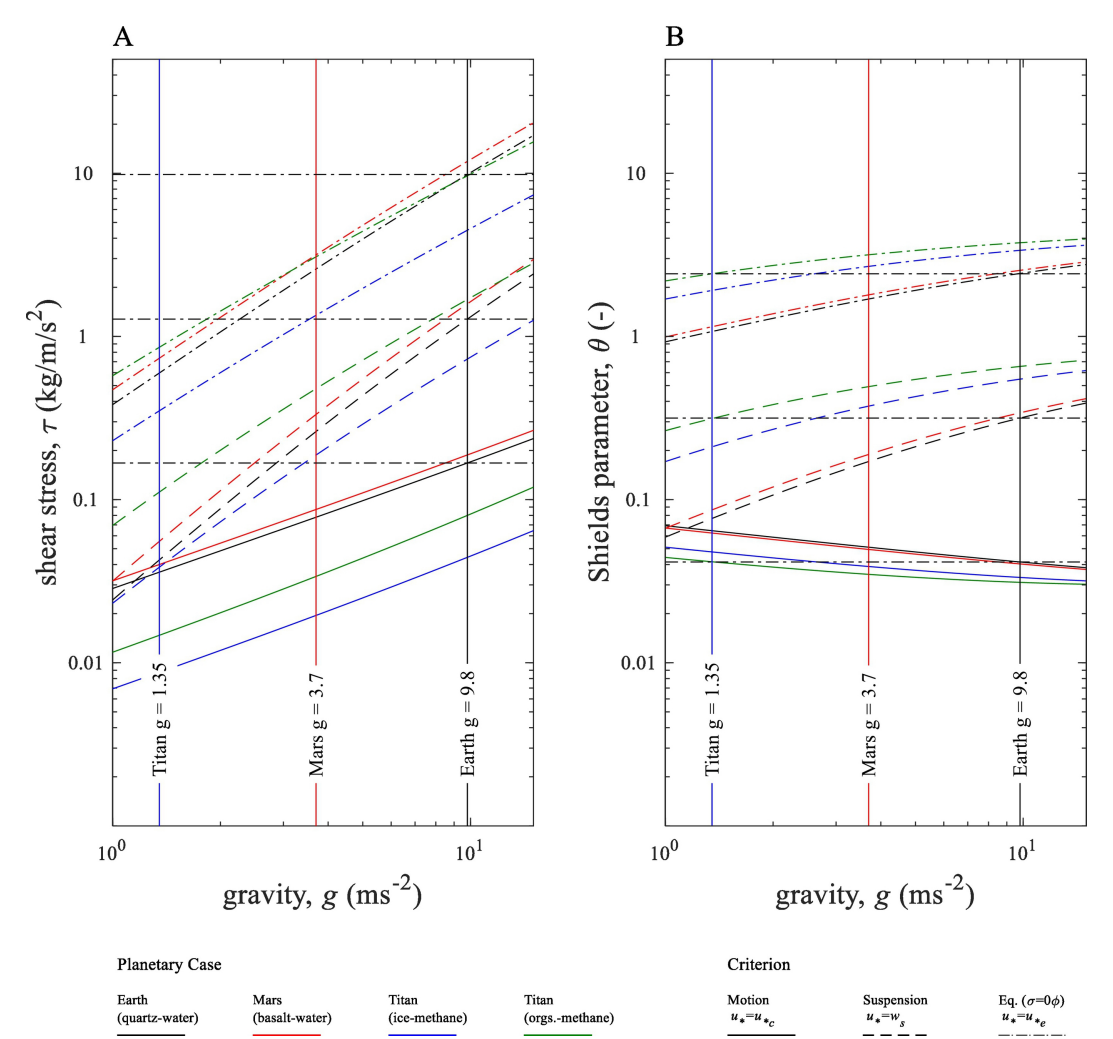
A
B
shear stress, τ (kg/m/s^2)
Shields parameter, θ (-)
10
1
0.1
0.01
Titan g = 1.35
Mars g = 3.7
Earth g = 9.8
10^0
10^1
gravity, g (ms^{-2})
Planetary Case
Earth (quartz-water)
Mars (basalt-water)
Titan (ice-methane)
Titan (orgs.-methane)
Criterion
Motion $u_*=u_{*_c}$
Suspension $u_*=w_s$
Eq. ($\sigma=0\phi$) $u_*=u_{*_e}$

Figure 7

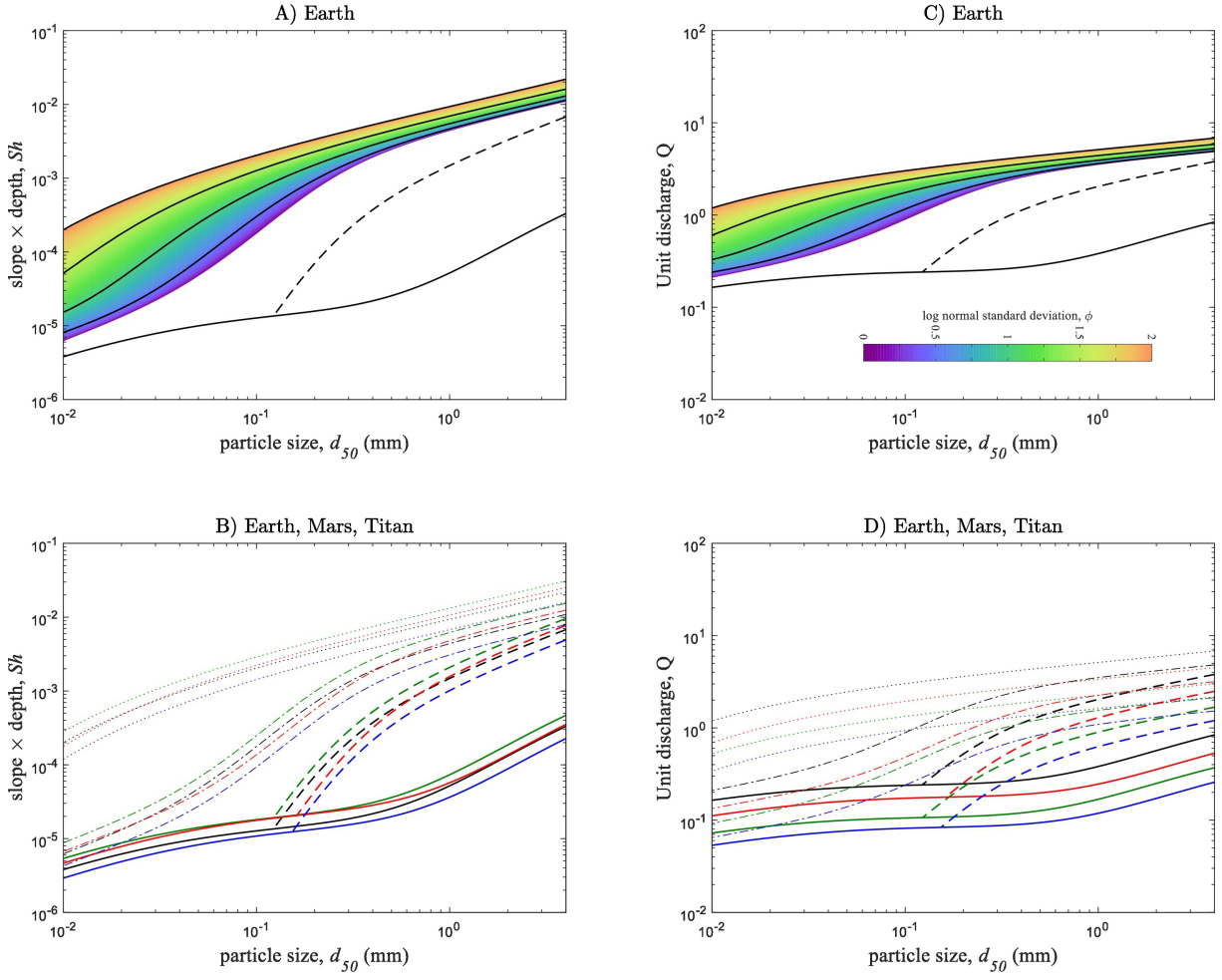
A) Earth
C) Earth
B) Earth, Mars, Titan
D) Earth, Mars, Titan
slope × depth, Sh
Unit discharge, Q
particle size, d_{50} (mm)
log normal standard deviation, ϕ
0
0.5
1
1.5
2
Planetary Case
Earth (quartz-water)
Mars (basalt-water)
Titan (ice-methane)
Titan (orgs.-methane)
Criterion
Motion $u_*=u_{*_c}$
Suspension $u_*=w_s$
Eq. ($\sigma=0\phi$) $u_*=u_{*_e}$
Eq. ($\sigma=2\phi$) $u_*=u_{*_e}$

Figure 8

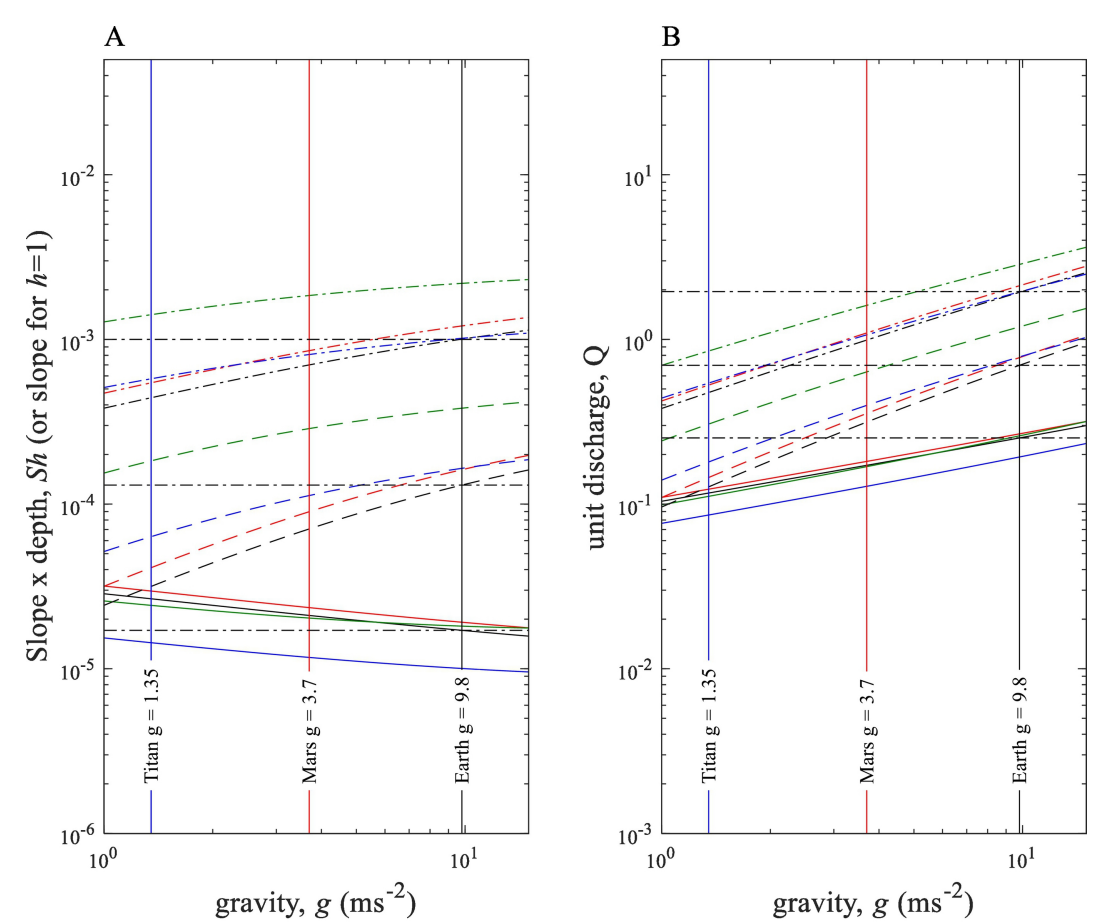
A
B
Slope x depth, Sh (or slope for h=1)
unit discharge, Q
gravity, g (ms-2)
gravity, g (ms-2)
Titan g = 1.35
Mars g = 3.7
Earth g = 9.8
Titan g = 1.35
Mars g = 3.7
Earth g = 9.8
Planetary Case
Earth (quartz-water)
Mars (basalt-water)
Titan (ice-methane)
Titan (orgs.-methane)
Criterion
Motion u*=u*c
Suspension u*=ws
Eq. (σ=0ϕ) u*=u*e

Figure 9

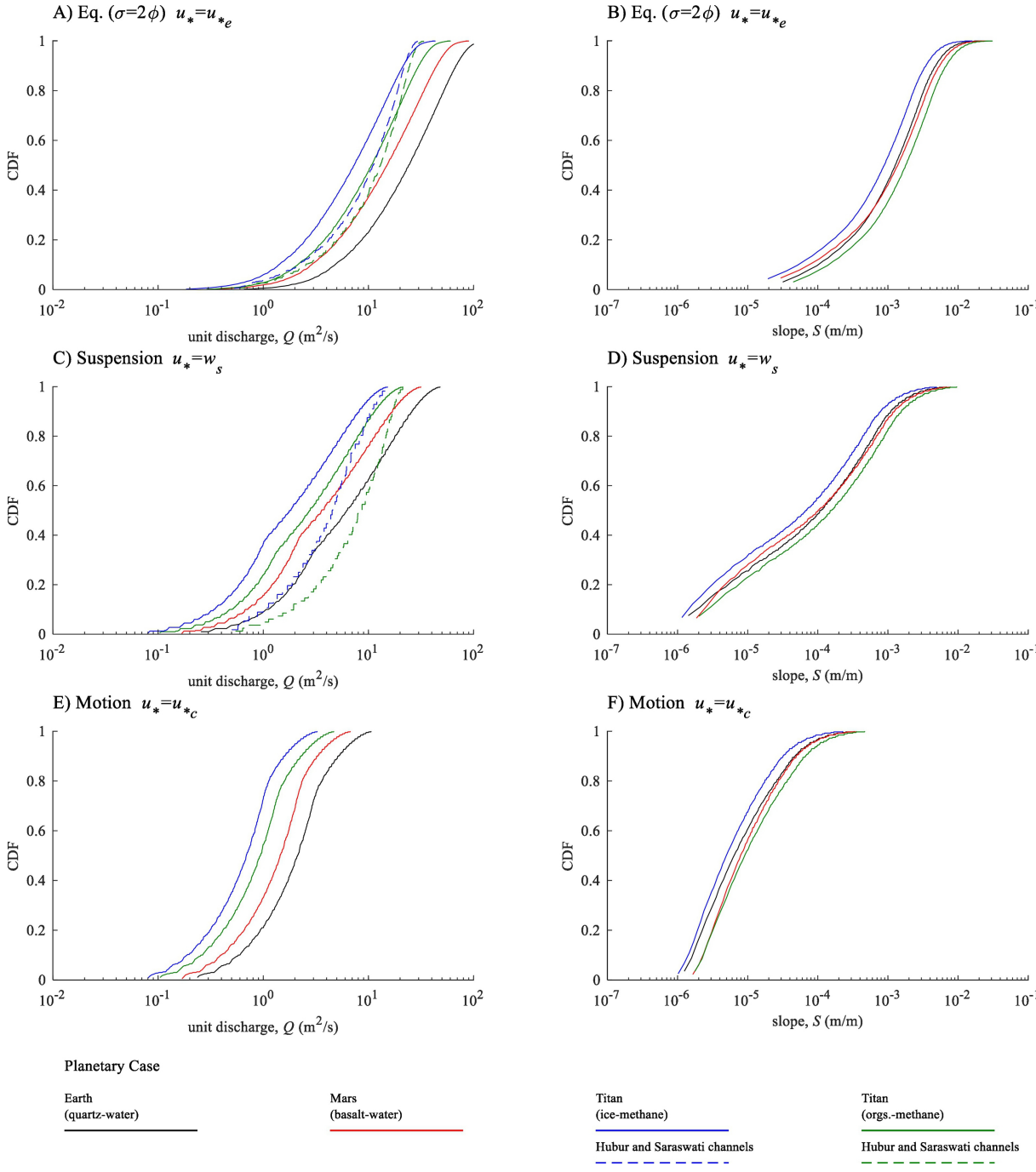
A) Eq. (σ=2ϕ) u_*=u_{*e}
B) Eq. (σ=2ϕ) u_*=u_{*e}
C) Suspension u_*=w_s
D) Suspension u_*=w_s
E) Motion u_*=u_{*c}
F) Motion u_*=u_{*c}
CDF
unit discharge, Q (m^2/s)
slope, S (m/m)
Planetary Case
Earth (quartz-water)
Mars (basalt-water)
Titan (ice-methane)
Titan (orgs.-methane)
Hubur and Saraswati channels
Hubur and Saraswati channels

Figure 10

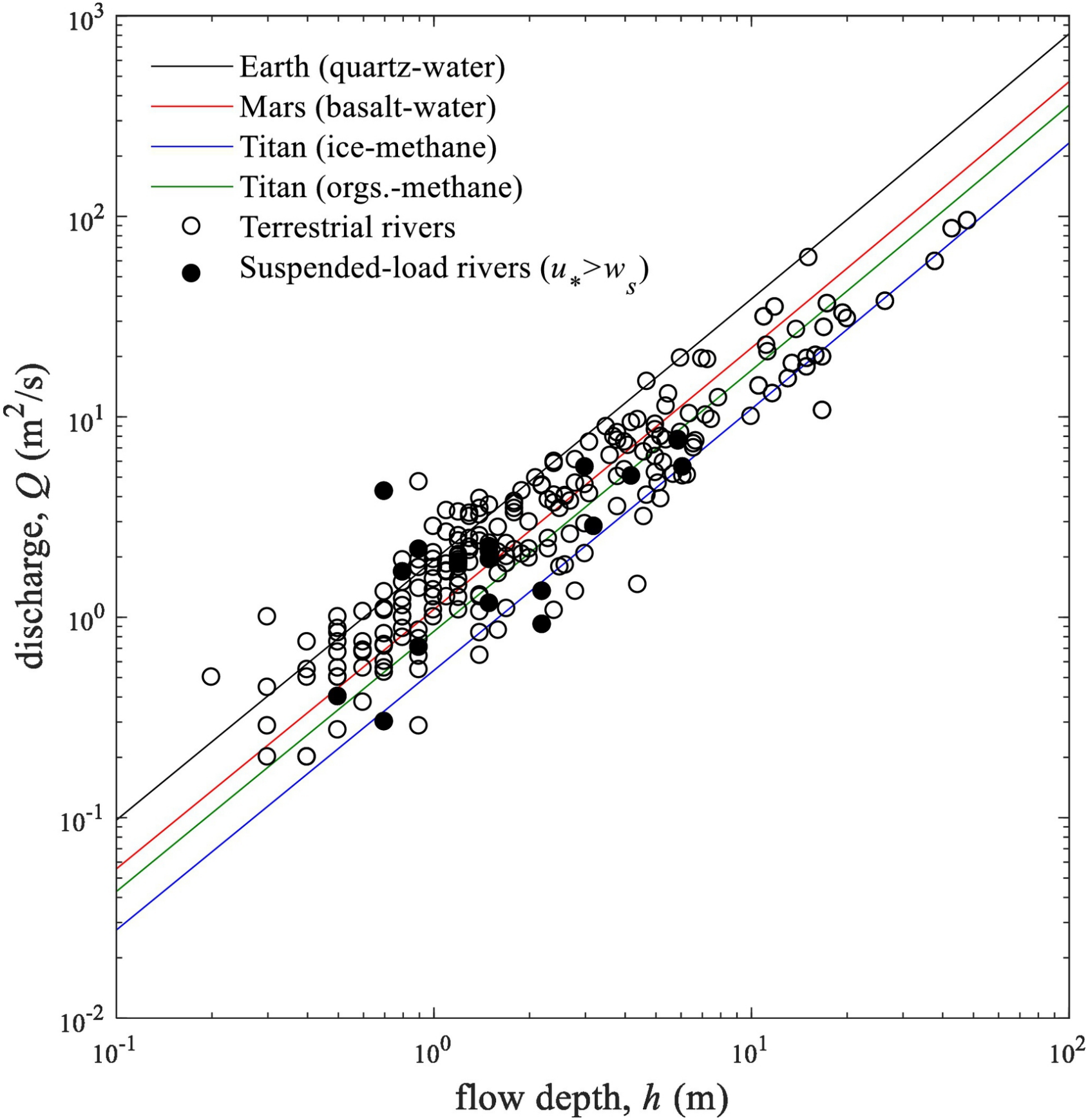
Earth (quartz-water)
Mars (basalt-water)
Titan (ice-methane)
Titan (orgs.-methane)
Terrestrial rivers
Suspended-load rivers ($u_* > w_s$)
discharge, Q (m^2/s)
flow depth, h (m)
10^{3}
10^{2}
10^{1}
10^{0}
10^{-1}
10^{-2}
10^{-1}
10^{0}
10^{1}
10^{2}

Figure 11